Title

Mechanistic insights into the catalytic methanol steam reforming performance of Cu/ZrO2 catalysts by in situ and operando studies

Authors

Ploner, Kevin
Watschinger, Maximilian
Nezhad, Parastoo Delir Kheyrollahi
et al.

Publication Date

2020-11-01

DOI

10.1016/j.jcat.2020.09.018

Peer reviewed

Mechanistic Insights into the Catalytic Methanol Steam Reforming Performance of Cu/ZrO_2 Catalysts by *In Situ* and *Operando* Studies

Kevin Ploner[1], Maximilian Watschinger[1], Parastoo Delir Kheyrollahi Nezhad[1], Thomas Götsch[1,2], Lukas Schlicker[3], Eva-Maria Köck[1], Aleksander Gurlo[3], Albert Gili[3], Andrew Doran[4], Lei Zhang[5], Nicolas Köwitsch[5], Marc Armbrüster[5], Stefan Vanicek[6], Wolfgang Wallisch[7], Christoph Thurner[1], Bernhard Klötzer[1] and Simon Penner[1,*]

[1]*Department of Physical Chemistry, University of Innsbruck, Innrain 52c, A-6020 Innsbruck, Austria*

[2]*Current address: Fritz Haber Institute of the Max Planck Society, Department of Inorganic Chemistry, Faradayweg 4-6, 14195 Berlin, Germany*

[3]*Chair of Advanced Ceramic Materials, Institut für Werkstoffwissenschaften und -technologien, Technical University Berlin, Hardenbergstr. 40, D-10623 Berlin, Germany*

[4]*Advanced Light Source, Lawrence Berkeley National Laboratory, Berkeley, California 94720, USA*

[5]*Institute of Chemistry, Materials for Innovative Energy Concepts, Technical University Chemnitz, Straße der Nationen 62, D-09111 Chemnitz, Germany*

[6]*Department of General, Inorganic and Theoretical Chemistry, University of Innsbruck, Innrain 80-82, A-6020 Innsbruck, Austria*

[7]*University Service Centre for Transmission Electron Microscopy, TU Wien, Wiedner Hauptstraße 8-10/057-02, A-1040 Vienna, Austria*

Keywords: copper; tetragonal zirconia; monoclinic zirconia; *in situ* X-ray diffraction; CO_2 selectivity; *in situ* FT-IR spectroscopy; *operando* DTA/TG

*Corresponding Author: simon.penner@uibk.ac.at, Tel: 004351250758003, Fax: 004351250758199

Abstract

We assessed the catalytic properties of the Cu/ZrO_2 interface in methanol and formaldehyde steam reforming (MSR and FSR) on powder catalysts by using a comparative approach with respect to the influence of the ZrO_2 polymorph support structure (monoclinic (m-)ZrO_2 *vs.* tetragonal (t-)ZrO_2), its synthesis routine and the choice of the precursor material on the CO_2 selectivity. Our studies reveal that ZrO_2 exhibits a pronounced versatility as a support material and its catalytic properties depend most strongly on its surface properties governed by its synthesis, especially by the choice of the Zr precursor. The way of combining the support with copper introduces an additional layer of complexity, but its influence on the MSR performance is limited to a modification of the conditions provided by the ZrO_2 support. Exploiting the comparative approach regarding the Cu-ZrO_2 catalysts in FSR and MSR – including the pure support materials – in combination with *in situ* Fourier transform infrared (FT-IR) spectroscopy shows that the CO observed in MSR on Cu/m-ZrO_2 can be attributed to a spillover of formaldehyde to the support. Side reactions of m-ZrO_2 are suppressed at lower temperatures due to its lack of highly reactive sites, resulting in a CO_2-selective MSR performance. In Cu/t-ZrO_2, however, the amount of CO is higher and a combination of a formaldehyde spillover to the support and a Cu-ZrO_2 phase boundary yielding CO leads to the lower CO_2 selectivity of these samples. An elevated number of defects and reactive Lewis acidic and Brønsted basic centers of t-ZrO_2 explains this increased activity towards side reactions in contrast to Cu/m-ZrO_2 catalysts.

1. Introduction

Methanol steam reforming (MSR) is one of the most important reactions in the hydrogen economy, as it allows to obtain high contents of hydrogen in the effluent if the reaction is steered toward maximum CO_2 selectivity.[1] The reaction equation of MSR[2] is given in Equation 1:

$$\mathrm{CH_3OH_{(g)} + H_2O_{(g)} \rightleftarrows 3\ H_{2,(g)} + CO_{2,(g)}} \qquad \Delta H_r^0 = 49.6\ \mathrm{kJ\ mol^{-1}} \qquad \text{Equation 1}$$

Potential side reactions are the methanol decomposition[2] (Equation 2), the reverse water-gas shift reaction[2] (Equation 3) and the methanation of CO or CO_2 toward methane[3] (Equations 4 and 5):

$$\mathrm{CH_3OH_{(g)} \rightleftarrows 2\ H_{2,(g)} + CO_{(g)}} \qquad \Delta H_r^0 = 90.6\ \mathrm{kJ\ mol^{-1}} \qquad \text{Equation 2}$$

$$\mathrm{CO_{2,(g)} + H_{2,(g)} \rightleftarrows H_2O_{(g)} + CO_{(g)}} \qquad \Delta H_r^0 = 41.1\ \mathrm{kJ\ mol^{-1}} \qquad \text{Equation 3}$$

$$\mathrm{CO_{2,(g)} + 4\ H_{2,(g)} \rightleftarrows CH_{4,(g)} + 2\ H_2O_{(g)}} \qquad \Delta H_r^0 = -165\ \mathrm{kJ\ mol^{-1}} \qquad \text{Equation 4}$$

$$\mathrm{CO_{(g)} + 3\ H_{2,(g)} \rightleftarrows CH_{4,(g)} + H_2O_{(g)}} \qquad \Delta H_r^0 = -206\ \mathrm{kJ\ mol^{-1}} \qquad \text{Equation 5}$$

The catalyst currently used in applications on a larger scale, $Cu/ZnO/Al_2O_3$, suffers from a number of drawbacks especially connected to pronounced Cu particle sintering resulting in unsatisfactory long-term performance.[4] Substitution of ZnO by a support material that is able to suppress copper particle sintering, such as ZrO_2, is one possibility to overcome these stability issues.[5–9] The preparation of $CuO/ZnO/Al_2O_3/ZrO_2$ systems in some reports leads to a better long-term stability compared to the ZrO_2-free catalysts.[5,6] However, the influence of ZrO_2 goes well beyond a simple structural stabilization of the Cu particles. Rather, synergistic bifunctional operation of metal and support[10] determines the beneficial effects of ZrO_2 promotion of Cu catalysts, which has been shown to lead to the formation of a

Cu/ZrO_2 compound with very promising catalytic behavior with respect to high CO_2 selectivity.[5–8] Nevertheless, predominantly in comparison to Cu/ZnO, the structural, electronic and chemical nature of Cu/ZrO_2 catalysts and interfaces becomes rather complicated due to the complex Zr-O phase diagram,[11,12] featuring three crystalline modifications of ZrO_2 at ambient pressure.[13] These encompass monoclinic (m-)ZrO_2 (room temperature to 1170 °C, space group $P2_1/c$)[14] as the thermodynamically stable low-temperature polymorph and the high-temperature polymorphs tetragonal (t-)ZrO_2 (1170-2370 °C, space group $P4_2/nmc$)[15] and cubic (c-)ZrO_2 (2370-2680 °C, space group $Fm\bar{3}m$)[16]. The latter two exhibit a phase width toward oxygen deficiency in the phase diagram[11,17] and can be stabilized under ambient conditions either by deliberate cationic or anionic doping or by particle size control.[13,18,19] The performance of Cu in contact with either of the phases is strikingly different and a matter of constant debate in the MSR as well as the methanol synthesis community owing to the extraordinary versatility of the bulk as well as the surface properties of ZrO_2.[20] Tada *et al.* showed that starting from a ternary $Cu_aZr_{1-a}O_b$ precursor, reduction led to the formation of Cu nanoparticles on amorphous ZrO_2, displaying superior performance in the hydrogenation of CO_2 to methanol compared to analogous systems using monoclinic or tetragonal zirconia[21,22]. While no particular synergistic action has been observed for Cu/m-ZrO_2 interfaces in several studies[9,23], it is reported that especially the contact area between Cu and t-ZrO_2 may exhibit active and CO_2-selective sites.[9,24] What sets the Cu/t-ZrO_2 apart from its m-ZrO_2-containing counterpart in chemical or structural detail is unclear up to now. Stability issues, including epitaxial stabilization effects, have been put forward,[25] but are insufficient to encompass all the catalytic details, given the strong variation of potential key parameters governing the CO_2 selectivity. Promotion of dynamic water activation under reaction conditions as a prerequisite for CO_2-selective methanol steam reforming is an obvious key criterion.[4] Studies of Cu-Zr bulk bimetallic pre-catalysts show that they form a strongly hydroxylated CO_2-selective Cu/t-

ZrO_2 interface *in situ* upon contact to the MSR reaction mixture at 350 °C.[25] The bulk structure of the respective polymorph is of minor importance compared to the intrinsic physico-chemical properties of a particular Cu-ZrO_2 interface structure, accessed *via* special synthesis routines that allow for reversible dynamic hydroxylation/dehydroxylation under reaction conditions. So far, these studies have been limited to Cu-Zr bimetallic layers and real/inverse Cu-ZrO_xH_y model systems.[25–27]

To close the material gap originating from model catalyst studies and to transfer mechanistic ideas to technically more relevant powder Cu-ZrO_2 catalyst systems in the presented work, we focus on selected Cu/ZrO_2 interfaces of varying surface and bulk properties of both Cu and ZrO_2 accessible by different preparation methods and support structures. As descriptors, we utilize (a) different ZrO_2 polymorphs (m-ZrO_2 and t-ZrO_2), (b) different synthesis pathways (Cu impregnation *vs.* Cu/Zr co-precipitation) and (c) different catalyst precursors (Zr/Cu isopropoxide *vs.* Cu acetate). Correlating the parameter space yields Cu/t-ZrO_2 and Cu/m-ZrO_2 materials that are treated under the exact same pre-treatment and reaction conditions and can, thus, be directly compared in terms of their catalytic performance in MSR. This ideally allows the correlation of the CO_2 selectivity with surface and bulk features of both Cu and ZrO_2. As a particular feature of the Zr-O system, the phase transformation of metastable t-ZrO_2 to m-ZrO_2 depending on the Zr precursor and gas atmosphere needs to be taken into account.[13,18,28]

Mapping the different descriptors enables us to focus on providing in-depth information on the reaction mechanism of Cu in contact with either ZrO_2 polymorph.

Cu-based catalysts are capable of producing formaldehyde from methanol in MSR,[29] as well as in the (partial) oxidation[30,31] and in decomposition reactions.[32–34] As the ultimate goal of the present work is to disentangle the surface and bulk parameters that control the overall catalytic performance of Cu-ZrO_2, valuable mechanistic insight is expected from starting the steam reforming reaction from different species in the methanol steam reforming

reaction axis and, at the same time, relating it to the performance of the pure ZrO_2 materials. Hence, starting the steam reforming reaction from formaldehyde as the main crossing point crucially influencing the CO_2 selectivity eliminates the necessity to activate methanol. This yields valuable information on the potential MSR reaction mechanism, especially with respect to materials that are potentially not capable of enabling this elementary reaction step. In this work, we exemplarily studied this particular reaction step for two representative catalysts in combination with the pure support materials to elucidate the impact of Cu on the proficiency of methanol activation and the influence of spillover of intermediates (*i.e.* formaldehyde) to ZrO_2, which will be judged by the formaldehyde steam reforming (FSR) performance of the pure support materials.

The combination of catalytic profiles in MSR and FSR, structural characterization by *in situ* X-ray diffraction, *in situ* FT-IR, dissociative N_2O adsorption, X-ray photoelectron spectroscopy (XPS) and *operando* DTA/TG ultimately allows to disentangle the individual contributions of critical parameters that control the overall catalytic performance of Cu-ZrO_2 and to both tentatively identify crucial reaction intermediates and to infer mechanistic details of the catalytic performance of Cu in contact with different ZrO_2 polymorphs.

2. Experimental

2.1. Preparation of the catalysts

The support materials are m-ZrO_2 (purchased from Alfa Aesar, 99.978%) as well as t-ZrO_2 prepared by a precipitation routine of Zr(IV) isopropoxide in isopropanol (for details see Kogler *et al.*[18]). The catalysts were successively obtained using two different copper precursors (copper(II) acetate and copper(II) isopropoxide) and three synthesis routines, being aqueous impregnation with copper acetate (with m- and t-ZrO_2), water-free impregnation with copper isopropoxide in isopropanol (with m- and t-ZrO_2) and co-precipitation of copper isopropoxide and zirconium isopropoxide (yielding t-ZrO_2). Details of the syntheses are

outlined in the Supporting Information (SI) in Section A. For a complete list of all samples including their copper loading after calcination as determined by ICP-OES, see Table 1. The nominal copper loading of all samples (except for the pure supports) amounts to 6.9 wt% Cu after pre-reduction. The ICP-OES experiments were validated by oxidation-reduction-oxidation experiments using thermogravimetric analysis (TGA, for details see SI, Section B) and essentially yielded similar values for the Cu loadings. Small differences arose due to minor solubility issues of the Cu phase in the ICP-OES experiment.

2.2. Catalytic measurements

Catalytic characterization is carried out in a dedicated recirculating batch reactor setup (detailed description see SI, Section B). The methanol steam reforming mixture is prepared as to obtain a composition of methanol:water = 1:2 in the gas phase to avoid the steam reforming reaction being stopped by water depletion. Several freeze-and-thaw cycles are performed prior to the catalytic measurements to degas the reaction mixture. A methanol steam reforming cycle consists of three steps: (1) pre-oxidation in 1 bar O_2 at 400 °C for 1 h (termed O400), (2) pre-reduction in 1 bar H_2 at 300 °C for 1 h (termed H300) and (3) MSR reaction. The latter consists of adding the reaction mixture (≈ 28 mbar) and defined amounts of Ar for baseline correction (to account for the gas withdrawal through the leak toward the quadrupole mass spectrometer (QMS)) to the reactor and backfilling the reactor with He to atmospheric pressure (to enhance the thermal conductivity and recirculation efficiency) at 100 °C. A temperature ramp from 100 °C to 350 °C with a rate of 5 °C min^{-1} is subsequently applied with continuous quantification by QMS.

The raw MS signals are converted to partial pressures using an external calibration for the gases H_2, CO, CO_2 and CH_4 with fragmentation correction (subtraction of fragments that superpose with signals used for quantification, *e.g.* the m/z = 28 fragment of CO_2 interferes with the m/z = 28 signal of CO). Additionally, the potential formation of formaldehyde or

formic acid is monitored, whereas a quantitative calibration is not feasible for these species in this setup. For direct comparison of the different activities and enabling relation to literature data, the partial pressures are converted to formation rates by differentiation of the signals and normalization to the total copper mass. Application of the ideal gas equation yields formation rates (or specific activity) in µmol g_{Cu}^{-1} s^{-1}, enabling direct comparison with literature.[35] The methanol conversion is calculated relative to the signal m/z = 31 at the start of the temperature ramp and the CO_2 selectivity S_{CO_2} is obtained with Equation 6 and the formation rates of CO_2 ($r(CO_2)$), CO ($r(CO)$) and CH_4 ($r(CH_4)$).

$$S_{CO_2} = \frac{r(CO_2)}{r(CO_2) + r(CO) + r(CH_4)} \qquad \text{Equation 6}$$

Formaldehyde steam reforming (FSR) was performed using a commercially available formaldehyde/water mixture (30% formaldehyde in water, methanol-free, Carl Roth GmbH, Karlsruhe) degassed with respect to dissolved O_2 by three freeze-and-thaw cycles. Utilizing the vapor pressure at room temperature (≈ 10 mbar total pressure) yields a formaldehyde:water ratio of approximately 1:4 in the gas phase. Adsorption/desorption equilibria at colder parts of the setup prevent a precise quantification of the pressure as well as the reliable calculation of the CH_2O conversion.

To determine the activation energies, the TOF values in 10^{-3} s^{-1} are plotted *vs.* the reaction temperature and the resulting profile is fitted with an Arrhenius function at the beginning of the rate increase (*i.e.* at conversion well below 10%). By simultaneous independent variation of both the activation energy E_A and the pre-exponential factor A, values ranging from $1.8 \cdot 10^6$ s^{-1} to $5.9 \cdot 10^7$ s^{-1} are obtained for the latter. For the sake of better relative comparability of the corresponding activation energies, a fixed value of $1 \cdot 10^7$ s^{-1} was used in our calculations.

The turnover frequency (TOF) values are obtained by estimating the number of active Cu surface sites. With the specific copper surface area after pre-reduction obtained from the dissociative N_2O adsorption, the total number of sites is calculated by multiplication with the number of Cu sites per m^{-2} ($1.46 \cdot 10^{19}$ m^{-2}, assuming an equal contribution of the (100), (110) and (111) surface planes[36]). Under the assumption that all accessible metallic Cu surface atoms are catalytically active, the resulting TOF values represent lower limits.

The mass and heat transfer limitations in the utilized recirculating batch reactor were considered and both found to be insignificant. The extent of the mass transport limitation was estimated as reported before for an analogous setup[37] by calculation of the collision number Z ($Z = p/(2\pi mkT)^{1/2}$; $Z = 1.1 \cdot 10^{22}$ cm^{-2} s^{-1}) and the maximum total CO_2 rate (sample number 1; $5.7 \cdot 10^{15}$ cm^{-2} s^{-1}). This comparison yields a collision number several orders of magnitudes larger than the maximum total rates of any gas involved in the reaction. Therefore, the diffusion limitation is negligible. The effect of heat transfer limitation is suppressed by the addition of an excess of helium displaying a high thermal conductivity.

Continuous flow tests were carried out in a fixed bed reactor system (PID Eng&Tech, Microactivity Reference) connected to a MicroGC (Varian CP 4900, equipped with a 10 m back-flushed M5A column, a 20 m back-flushed M5A colum and a 10 m PPU column, Agilent Technologies) for the simultaneous analysis of H_2, CH_4, CO and CO_2. The samples were mixed with graphite (ChemPur, < 100 µm, 99.9%) as dilutant to ensure homogenous gas flow through the sample and placed in the reactor tube (stainless steel coated with silicon oxide, inner diameter 7.9 mm) on top of a quartz fleece. The material was pre-treated according to the DTA/TG/MS results *in situ* (see section 2.5). For the catalytic tests a mixture of 10% He/N_2 (45 ml min^{-1}, Air Liquide, 99.999%) was used as carrier gas which was mixed with a H_2O/MeOH vapor (0.01 ml min^{-1} $H_2O_{(l)}$, 0.0225 ml min^{-1} $MeOH_{(l)}$, Fisher Scientific, HPLC grade). The liquid vapors were condensed in a cooling trap and the gas stream was further dried by a Nafion® membrane, which was dried in counter flow by a N_2-flow of

100 ml min^{-1}. The dry gas stream was then analyzed by online gas chromatography to determine the formation rates employing the ideal gas equation and the CO_2 selectivity according to Equation 6.

2.3. Structural characterization

The bulk structural changes of the ZrO_2-supported Cu specimens during the catalytic process were studied *via* time-resolved *in situ* synchrotron XRD measurements at the beamline 12.2.2 at the Advanced Light Source (ALS) at the Lawrence Berkeley National Laboratory (LBNL), California. X-ray diffraction was performed in transmission mode with a monochromatic 25 keV beam with a spot size of 30 µm. A Perkin Elmer image plate detector was used to record one pattern per 180 s. The sample-to-detector distance, the detector tilt and the exact wavelength (0.4971 Å) were calibrated with a LaB_6 NIST standard in the Dioptas software, which was also employed for integration of the two-dimensional detector images.[38]

Two complete cycles of (i) oxidation 400 °C for 60 min (ii) reduction at 300 °C for 60 min and (iii) MSR from 120-350 °C with a heating rate of 10 °C min^{-1} and an additional isothermal period for 20 min were conducted with several samples of Cu supported on t-ZrO_2 and m-ZrO_2. The specimen powders mounted in capillaries (diameter 700 µm) were heated with an infrared capillary furnace,[39] while the required gaseous environment for the subsequent oxidation and reduction steps was provided as described earlier[40] using pure oxygen and hydrogen in flow-through mode.

To perform the *in situ* measurements, a gas phase methanol steam reforming mixture (methanol:water = 1:2) was seeded in He carrier gas and passed through a heated pipe to prevent condensation into the sample capillary. The experiments were performed in quasi flow-through conditions. The pure He for subsequent cooling (after MSR) was provided through a separate clean pipe, in this manner bypassing the methanol:water vessel and preventing the introduction of steam into the system.

BET measurements were performed with a NOVA 2000e Surface Area & Pore Size Analyzer (Quantachrome Instruments) using the software Quantachrome NovaWin. Sample pretreatment involved heating to 200 °C *in vacuo* for 30 min followed by adsorption of N_2 at -196 °C at five points from 0.05 to 0.30 p/p_0.

2.4. *In situ* spectroscopic characterization by FT-IR

Fourier transform infrared (FT-IR) spectra were recorded in transmission mode using an Agilent Cary 660 spectrometer with a mid-infrared source and a DTGS detector. The powder samples were pressed into thin pellets using a pressure of 2 t (10 mm diameter, ≈ 0.1 mm thick, sample mass about 10 mg) and subsequently placed inside a home-built reactor cell, providing a chemically inert environment for the sample in the heated area and allowing *in situ* measurements up to 1000 °C under flowing and static conditions.[41] Desorption measurements in vacuum with a minimum pressure of $2 \cdot 10^{-7}$ mbar were also conducted. The window material BaF_2 allows to access wavelengths above 800 cm^{-1}. Methanol steam reforming was performed as described before according to the catalytic reactivity measurements, *i.e.* utilizing the gas phase over a liquid mixture of methanol:water = 1:10 in batch reactor configuration.

2.5. Differential thermal analysis/thermogravimetry/mass spectrometry measurements (DTA/TG/MS)

DTA/TG/MS measurements were conducted under MSR conditions. Therefore, a defined amount of powdered material was measured in Al_2O_3 crucibles in a Netzsch STA 449 F3 Jupiter DTA/TG. The specific mass/charge-signals of the outgoing gases were surveyed with a mass spectrometer (Pfeiffer, Omnistar GSD 301 O3). The *operando* DTA/TG measurements were performed in a way to closely resemble the *in situ* XRD experiments, *i.e.* pre-oxidation and pre-reduction were also performed prior to the actual MSR experiment. The materials

were then kept under He flow (40 ml min^{-1}) for 30 min to get a stable baseline, and subsequently heated to 150 °C with a rate of 5 °C min^{-1} and kept at that temperature for 30 min. Then a flow of 0.39 g h^{-1} liquid MeOH/H_2O-mixture (50 mol-% methanol (Fisher Scientific, HPLC grade), 50 mol-% deionized water) was evaporated at 200 °C and added to the gas mixture. After that, the sample was heated to 350 °C with a rate of 5 °C min^{-1}, held there isothermally for 30 min, cooled to 150 °C with 5 °C min^{-1} and held there again for 30 min. This heating and cooling cycle was repeated to investigate if the changes on the sample are reversible. Then the flow of MeOH/H_2O was stopped and the material was cooled to room temperature in helium. The individual measurements are background corrected by means of a blind measurement of the empty Al_2O_3 crucibles.

2.6. Dissociative N_2O adsorption

Metallic copper can be selectively oxidized at the surface to Cu_2O with N_2O for the determination of the accessible copper surface area. [36,42,43] The effective volume of the reactor including the loaded sample was determined *via* expansion of He (5.0, Messer) from a calibrated manifold volume at 300 °C. The samples were reduced in pure flowing H_2 (5.0, Messer) at 300 °C for 30 min, yielding metallic copper. This procedure was followed by evacuation, purging with He and additional evacuation. The catalysts were cooled down *in vacuo* to 70 °C and a defined pressure of N_2O (2.0, Messer) monitored by a Baratron pressure transducer (MKS Instruments) was provided in the manifold. The consumption of N_2O and the formation of N_2 was monitored for 90 min by a quadrupole mass spectrometer (QMS) from Balzers (QMA125; QME 125-9) after opening the valve to the sample. After evacuation and flushing with He, the temperature was increased to 300 °C. A defined amount of H_2 calculated with the ideal gas law was provided in the manifold and the pressure decrease upon reduction of the newly formed surface Cu_2O was observed over the course of 35 min. Using the He-calibration and the so obtained effective volume at 300 °C, the molar amount of H_2

consumed can be calculated with the ideal gas law once more. The consumed molar amount of hydrogen n_{H_2} (see Equation 7) is calculated as the difference between the amount supplied in the manifold at room temperature and the remaining amount in the effective sample volume at 300 °C.

$$n_{H_2} = \frac{p_{man} * V_{man}}{R * T_{man}} - \frac{p_{sample} * V_{eff}}{R * T_{sample}} \qquad \text{Equation 7}$$

where n_{H_2} is the amount of hydrogen (in mol) consumed during reduction, p_{man} is the pressure in the manifold (in Pa), V_{man} is the calibrated volume of the manifold (in m^3), R is the ideal gas constant (= 8.3145 J mol^{-1} K^{-1}), T_{man} is the temperature in the manifold (= 298 K), p_{sample} is the pressure after hydrogen consumption in the reactor (in Pa), V_{eff} is the effective volume considering the temperature gradient in the reactor at T_{sample} (in m^3), T_{sample} is the sample temperature (in K).

The consumed amount of H_2 is equivalent to twice the amount of Cu surface atoms, since the reduction of 1 mol of (surface) Cu_2O with H_2 yields 2 mol of Cu^0. Utilizing this information, the specific copper surface area SA_{Cu} and the dispersion D_{Cu} can be calculated using Equation 8 and Equation 9, respectively.[43]

$$SA_{Cu}\ (m^2 / g_{Cat}) = \frac{2 * n_{H_2} * N_A}{SD_{Cu} * m_{Cat}} \qquad \text{Equation 8}$$

where SA_{Cu} is the specific Cu surface area (in m^2 g_{Cat}^{-1}), N_A is Avogadro's number (= $6.022 \cdot 10^{23}$ mol^{-1}), SD_{Cu} is the atom surface density of Cu (= $1.46 \cdot 10^{19}$ m^{-2})[36], m_{Cat} is the mass of catalyst used in the analysis (in g).

$$D_{Cu} = \frac{2 * n_{H_2} * M_{Cu}}{m_{Cu}} * 100 \qquad \text{Equation 9}$$

where D_{Cu} is the dispersion of Cu (in %), M_{Cu} is the molar mass of Cu (= 63.546 g mol^{-1}), m_{Cu} is the mass of Cu used in the analysis (in g).

2.7. X-ray photoelectron spectroscopy (XPS)

The chemical state of the sample surface was investigated with XPS utilizing a Thermo Scientific MultiLab 2000 spectrometer. It is equipped with a monochromatic Al K_α X-ray source and an Alpha 110 hemispherical sector analyzer. The base pressure lies in the low 10^{-9} mbar range and charging of the sample upon irradiation is compensated by a flood gun supplying electrons with a kinetic energy of 6 eV.

The purity of the samples was confirmed with survey scans and the detailed regions were recorded with a pass energy of 20 eV and an energy step size of 0.05 eV. Quantification of the surface composition was conducted using the Zr 3d, Cu $2p_{3/2}$, O 1s and C 1s regions and considering their relative sensitivity factors (RSFs)[44] as well as their inelastic mean free path with the G1 predictive formula according to Gries.[45] A Shirley function was employed to account for the background.

The qualitative assignment of the copper species was accomplished by comparison with Cu reference samples measured in the same instrument, namely metallic Cu (sputter-cleaned Cu foil, Goodfellow, 99.99+%), Cu_2O (Sigma-Aldrich, anhydrous, ≥99.99% trace metals basis), CuO (Sigma-Aldrich, 99.999% trace metals basis) and $Cu(OH)_2$ (synthesized by precipitation with $CuSO_4 \cdot 5\ H_2O$ (Merck, for analysis, 99.7%) and NaOH (Roth, ≥99%)).

2.8. Inductively coupled plasma optical emission spectroscopy (ICP-OES)

The chemical composition of the materials was obtained by ICP-OES (Varian Vista RL). The sample was dissolved in freshly prepared aqua regia (hydrochloric acid, 37%, nitric acid, 68%, VWR chemicals AnalaR NORMAPUR) diluted to 5% with water. Calibration was performed by dilution of the standard solutions to get a regression line for the concentration in the range of 20-100 mg l^{-1}.

3. Results and discussion

For the sake of clarity, an overview of the various studied systems is given in Table 1. On the basis of the seven samples, we explore the parameter space needed to judge the catalytic performance of different Cu/ZrO_2 materials. Note that the focus of the work is on disentangling the different intrinsic parameters steering the catalytic performance of the individual $Cu\text{-}ZrO_2$ to reveal a bigger picture of the selectivity-property relationships rather than maximizing the activity.

Table 1: Overview of the studied samples.

Preparation method and materials	Support material after calcination	Copper loading from ICP-OES / wt%	Acronym[a]
$Cu(OAc)_2$ impregnation of m-ZrO_2	m-ZrO_2	6.7	CmZAc-imp7
$Cu(OAc)_2$ impregnation of $Zr(OH)_4$-xerogel	t-ZrO_2	5.7[b]	CtZAc-imp7
$Cu(iPrO)_2$ impregnation of m-ZrO_2	m-ZrO_2	9.7[b]	CmZiPr-imp7
$Cu(iPrO)_2$ impregnation of $Zr(OH)_4$-xerogel	t-ZrO_2	7.3	CtZiPr-imp7
Co-precipitation of $Cu(iPrO)_2$ and $Zr(iPrO)_4$	t-ZrO_2	4.4	CtZiPr-copr7
m-ZrO_2 (purchased from Alfa Aesar)	m-ZrO_2	-	mZ
Precipitation of $Zr(iPrO)_4$	t-ZrO_2	-	tZ

[a]Explanations: C = Cu; mZ or tZ = monoclinic or tetragonal ZrO_2; Ac-imp = copper acetate impregnation, iPr-imp = copper isopropoxide impregnation, iPr-copr = co-precipitation of copper and zirconium isopropoxide; the number refers to the nominal copper loading after pre-reduction; [b]value determined *via* oxidation-reduction-oxidation DTA-TG measurements

3.1 Determination of the copper surface area by dissociative N_2O adsorption

The accessible copper surface area of the catalysts including the copper dispersion are listed in Table 2. The trend of the BET surface area is directly reflected in the Cu surface area, as CmZAc-imp7 exhibits the lowest and CtZAc-imp7 the highest value for both parameters, respectively. Generally, the systems with m-ZrO_2 as the support polymorph display a low surface area and copper dispersion, in contrast to the catalysts with t-ZrO_2. These observations

agree with the logical concept that a support with a high specific surface area leads to a high dispersion in an impregnation routine.

Table 2: BET surface area, accessible copper surface area and dispersion of the copper-containing samples.

Sample	BET surface area / $m^2\ g_{Cat}^{-1}$	SA_{Cu} / $m^2\ g_{Cat}^{-1}$	D_{Cu} / %
CmZAc-imp7	2	0.2	0.5
CmZiPr-imp7	3	0.5	0.8
CtZAc-imp7	143	2.7	7.2
CtZiPr-imp7	67	1.5	3.1
CtZiPr-copr7	89	1.3	4.5

3.2 Chemical characterization of the catalyst surface by XPS

For the determination of the surface composition and the chemical state of copper, *ex situ* XPS measurements were conducted after calcination and after MSR up to a final temperature of 350 °C. The atomic ratios of Cu/Zr in both states are listed in Table 3. Generally, a trend of an increased surface Cu/Zr ratio after MSR can be observed. The exception is CtZiPr-imp7, where this value decreases slightly. The Cu/Zr ratio in CmZiPr-imp7 is rather high in comparison to the other systems, but this can be explained by the low BET surface area in combination with a higher specific copper surface are compared to CmZAc-imp7. This means that the fixed amount of copper, which is comparable in all systems, is more likely able to cover a lot of the support, if its surface area is lower. Hence, the low Cu/Zr ratios of CtZAc-imp7 and CtZiPr-copr7 are a result of their high BET surface area of the t-ZrO_2 support, that cannot be covered entirely by the provided amount of copper.

Table 3: Surface composition determined by XPS after calcination and after MSR.

		CmZAc-imp7	CmZiPr-imp7	CtZAc-imp7	CtZiPr-imp7	CtZiPr-copr7
Atomic Cu/Zr ratio	After calcination	0.5	2.3	0.1	1.4	0.4
	After MSR350	0.7	4.7	0.3	1.2	0.8

The Cu 2p and Cu LMM regions of the five catalysts are depicted in Figure 1 together with reference samples of Cu, Cu_2O, CuO and $Cu(OH)_2$ measured at the same instrument. All of the Cu 2p regions exhibit the satellite feature, which is indicative for Cu^{2+} species.[46] The peak maxima after calcination are located between the CuO and $Cu(OH)_2$ reference samples, which hints to a mixture of these two species as the main copper components. This is expected after calcination and due to exposure to air during the sample transfer from the batch reactor to the XPS, slight reoxidation can be expected. Generally, the binding energy of the $2p_{3/2}$ peak is shifted to lower values and the satellite feature is less intense after MSR, which suggests a more reduced state of Cu.

The Cu LMM region shows a similar trend, albeit with less pronounced differences before and after MSR. The peak binding energy suggests either $Cu(OH)_2$ or Cu_2O for all samples, but the shape suggests the former to be the predominant species. The higher degree of hydroxylation indicated by the Cu LMM region can be explained by the higher information depth of these electrons due to their higher kinetic energy compared to the Cu 2p region. Since the hydroxide species is not stable in ultrahigh vacuum (as observed for the $Cu(OH)_2$ sample, which changed its color after prolonged storage in the XPS chamber in contrast to storage for the same time at ambient conditions), its concentration is expected to be higher in deeper regions of the sample due to a slower decomposition of the hydroxide species.

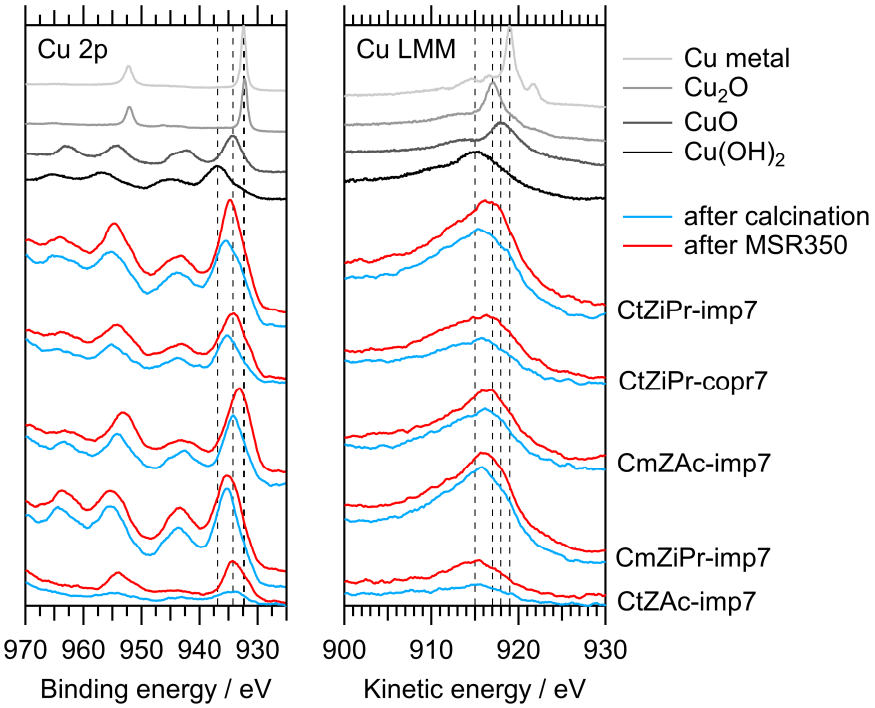

Figure 1: XP spectra of the Cu 2p and Cu LMM region of the catalysts after calcination and after MSR up to 350 °C. Additionally, reference samples of Cu, Cu_2O, CuO and $Cu(OH)_2$ were measured for qualitative assignment of the copper species.

3.3 Insights into the catalytic methanol steam reforming performance of Cu-ZrO_2 by using different ZrO_2 polymorphs: Cu acetate impregnation on m-ZrO_2 and t-ZrO_2

To deduce the individual MSR properties of m-ZrO_2 and t-ZrO_2, the pure support materials were subjected to the identical pre-treatments (O400 and H300) and equally characterized in methanol steam reforming (see SI Figure S2). As the total formation rates are smaller by 2-3 orders of magnitude compared to the Cu-containing samples, they are considered negligible. Both ZrO_2 polymorphs produce mainly CO and H_2 (ratio approximately 1:1) with t-ZrO_2 exhibiting additional formation of CO_2 traces and CH_4.

In addition to the differences in MSR performance, the defect chemistry and hydroxylation degree have been shown to be different for the two polymorphs. The observed ocher color of t-ZrO_2, in contrast to the purely white m-ZrO_2 (see SI Figure S1), is generally ascribed to the

formation of color center defects in YSZ and t-ZrO_2.[47–49]. Additionally, FT-IR investigations of Köck *et al.* on annealed m-ZrO_2 (same material as mZ) showed that it merely exhibits an extremely small amount of reversibly chemisorbed water, as well as little interaction with CO and CO_2 probe molecules.[50,51] Furthermore, they observed that t-ZrO_2 (prepared analogously to tZ in this study) is highly defective and shows Lewis acidic as well as Brønsted basic OH surface sites, which can be deduced from the formation of formates and carbonates with CO and CO_2 in FT-IR studies.[52] These strikingly different observations suggest a considerably higher reactivity of t-ZrO_2, which could explain the CO_2 and CH_4 formation on the Cu-free material necessarily requiring a certain ability of methanol and water activation.

3.3.1 Methanol and formaldehyde steam reforming performance of Cu-ZrO_2 starting from different ZrO_2 polymorphs

To directly compare Cu on m-ZrO_2 and t-ZrO_2 using identical preparation conditions with respect to catalyst synthesis (*i.e.* Cu impregnation), this section highlights the experiments of Cu acetate impregnation on either of the ZrO_2 polymorphs. Together with the *in situ* XRD and FT-IR studies (also on the pure ZrO_2 supports), this enables us to assess the catalytic performance and influence of selected ZrO_2 polymorphs without distortion of potentially different catalyst precursors or synthesis routines (which directly alter the surface properties of support and Cu-ZrO_2 interface). The MSR performance of CmZAc-imp7 in the first cycle is highlighted in Figure 2 Panel A (see SI Figure S3 for three consecutive MSR cycles). The onset temperatures of hydrogen and carbon dioxide formation are comparable at 150 °C and 165 °C, respectively. Carbon monoxide evolution starts 240 °C, resulting in almost 100% CO_2 selectivity up to this temperature. Due to the reactant limitation, the formation rates start to decline at around 310 °C. The mass balance of the products fits the MSR stoichiometry well over the whole reaction profile. At elevated temperatures, a small contribution of either

methanol dehydrogenation toward CO or the reverse water-gas shift reaction is superimposed. The evolution of the copper bulk structure is indicated by a colored background, which will be focused upon in more detail in section 3.3.2.

The isothermal long-term MSR measurement at 300 °C depicted in Figure 2 Panel B reveals that the selectivity toward CO_2 never drops below 90% and even increases once more to approximately 95% after 160 h. After 10 h, deactivation decreases the formation rates and the methanol conversion to about 25% of their maximum value, which can tentatively be ascribed to copper particle sintering. Based on the observed MSR profile, CmZAc-imp7 is considered the catalyst exhibiting the qualitatively most desirable performance of all studied systems with the same nominal Cu loading. In accordance, the Arrhenius fit of the CO_2 formation rate yields the smallest activation energy of ≈ 93 kJ mol^{-1} for this particular catalyst.

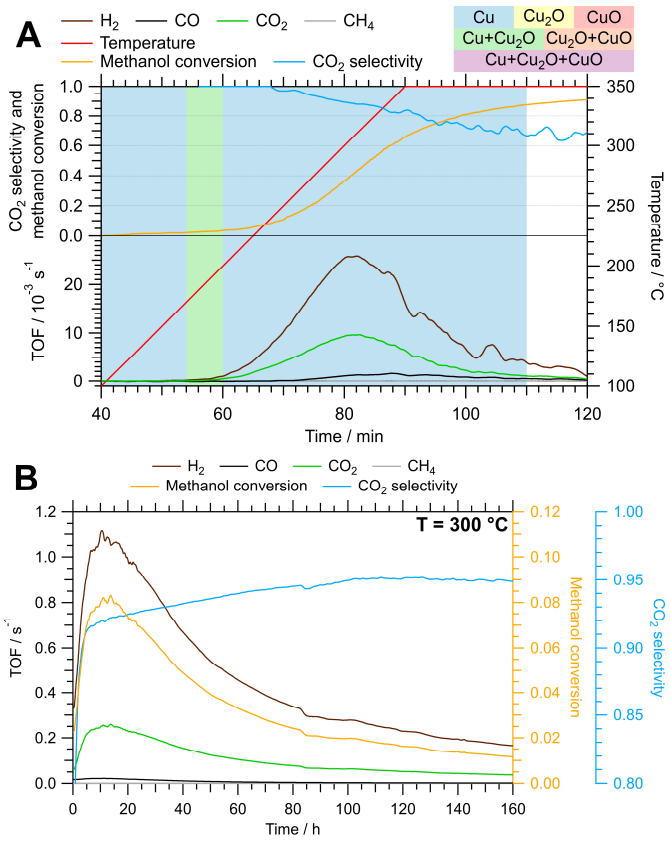

Figure 2: Panel A: Methanol steam reforming profile of CmZAc-imp7 between 100 °C and 350 °C. Color code: orange - methanol conversion, blue - CO_2 selectivity, formation rates of

brown: H_2, black: CO, green: CO_2, gray: CH_4. The temperature regions of the involved bulk Cu phases, as determined by *in situ* XRD (*cf.* Figure 5), are indicated by a colored background (see legend). Sample mass: 86.8 mg, heating rate: 5 °C min^{-1}. Panel B: Isothermal long-term catalytic MSR profile at 300 °C in a continuous flow reactor with a GHSV of 5500 h^{-1}; color code as in Panel A. Sample mass: 500.6 mg.

Formaldehyde steam reforming (FSR) was performed on both pure m-ZrO_2 and CmZAc-imp7 to enable a more reliable interpretation of the interface-specific reaction mechanism on these systems (Figure 3). The occurrence of formaldehyde as crucial intermediate in MSR is further supported by the similar apparent activation energies for CO_2 formation in MSR (≈ 84 kJ mol^{-1}) and in FSR (≈ 82 kJ mol^{-1}, both values were determined from the activity in µmol g_{Cu}^{-1} s^{-1} for better comparability). The CO formation rate of pure m-ZrO_2 in FSR is one order of magnitude higher compared to MSR (see SI Figure S2) and the light-off temperature is decreased from 300 to 250 °C. Additionally, around 200 °C CO_2 formation is observed, which subsides in the beginning of the isothermal period. This can be explained by the formation of stable adsorbates already at 100 °C, when the formaldehyde/water reaction mixture is applied, and their subsequent decomposition upon heating. The same phenomenon, but even more pronounced, can be observed for CmZAc-imp7 (Figure 3 Panel B), where the CO_2 formation stabilizes according to the FSR reaction. At low CO/CO_2 formation rates, the CO_2 selectivity cannot be quantified reliably. A dashed line represents the extrapolated reasonable value. The same extrapolation was performed for regions, where the selectivity pattern stabilizes after super-stoichiometric formation of one compound. Compared to MSR on CmZAc-imp7, the light-off temperature of H_2 is shifted from 150 to 200 °C, but apart from these two features, the catalytic profiles in MSR and FSR are very similar. The rates of CO formation on pure m-ZrO_2 and the catalyst containing copper in FSR are in the same range, in contrast to their performance in MSR, where CmZAc-imp7 produces much more CO than pure m-ZrO_2. These

observations lead to the conclusion that most of the carbon monoxide visible in MSR on CmZAc-imp7 could be produced by a spillover of formaldehyde species, which are formed from methanol activated by copper (or the phase boundary of Cu and ZrO_2), to the support. Since m-ZrO_2 yields CO from formaldehyde, this spillover would result in the formation of CO. The requirements for a CO_2-selective temperature range are therefore characterized by the capability to activate methanol, but inhibition of the spillover of formaldehyde species to the support.

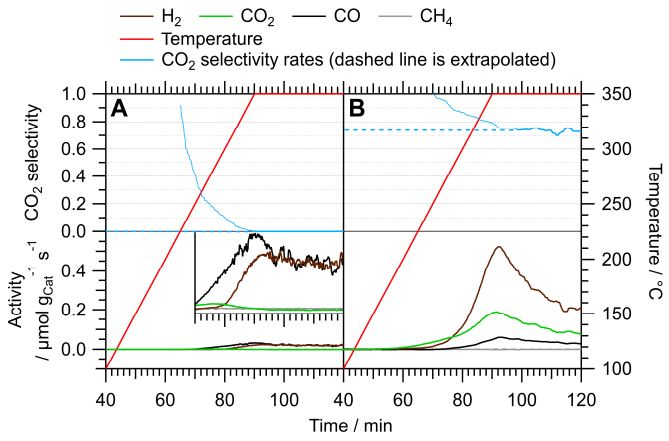

Figure 3: Panel A: Formaldehyde steam reforming profile on pure m-ZrO_2 (sample mass 101.4 mg) including a zoomed in region of the formation rates. Panel B: Formaldehyde steam reforming profile on CmZAc-imp7 (Panel B, sample mass: 27.5 mg) between 100 °C and 350 °C. Color code: blue - CO_2 selectivity, formation rates of brown: H_2, black: CO, green: CO_2, gray: CH_4. Heating rate: 5 °C min^{-1}.

By utilizing the same Cu impregnation method on the tetragonal ZrO_2 polymorph (CtZAc-imp7), a direct comparison of the catalytic performance in MSR is possible. Higher light-off temperatures of 210 °C for H_2 and 270 °C for CO and CO_2 are observed for this system (see Figure 4). These onset temperatures slightly shift to lower values in the second and third cycle by approximately 20 °C (see SI Figure S4). In essence, this catalyst is not CO_2-selective.

Formation of excess hydrogen, starting at considerably lower temperatures than CO_2, is observed, which is a common leading theme of all t-ZrO_2-containing systems (*cf.* also Figure 9 and 10). This is directly related to the capability of t-ZrO_2 to store dissolved hydrogen from the pre-reduction as demonstrated by Köck *et al.*[52] At significant formation rates, the rather poor selectivity toward carbon dioxide decreases to ≈ 50%. The apparent final increase to 100% is an artifact and originates from the decline of the formation rates to zero at about 100 min, because the reaction reaches its thermodynamic equilibrium. This is considered by the extrapolation of the CO_2 selectivity at significant CO/CO_2 rates to the region, where the formation rates of both products approach zero (dashed blue lines in Figure 4). Additionally, the Cu phase/redox evolution of CtZAc-imp7 in MSR is much more complex (indicated by the color-variable background in Figure 4 compared to Figure 2). This is discussed in detail at the end of section 3.3.2.

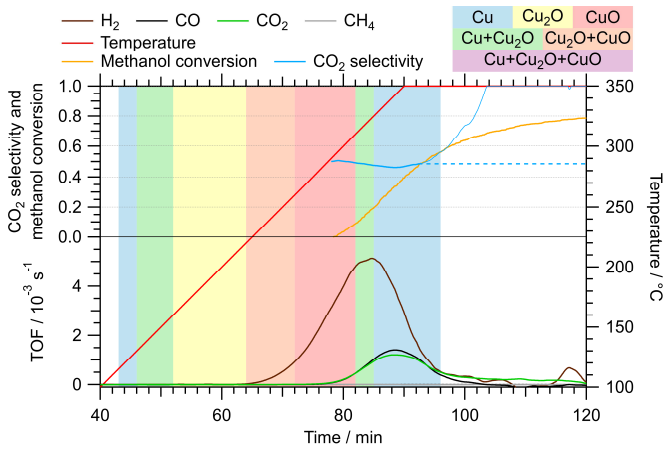

Figure 4: Methanol steam reforming profile of CtZAc-imp7 between 100 °C and 350 °C. Color code: orange - methanol conversion, blue - CO_2 selectivity, formation rates of brown: H_2, black: CO, green: CO_2, gray: CH_4. The temperature regions of the involved bulk Cu phases as determined by *in situ* XRD (*cf.* Figure S12) are indicated by a colored background (see legend). Heating rate: 5 °C min^{-1}; sample mass: 78.0 mg. The dashed blue line shows the extrapolated CO_2 selectivity to the region of low formation rates using the last significant value.

3.3.2 Determination of the bulk structural features of Cu-ZrO_2 (Cu acetate impregnation) by in situ XRD and operando DTA/TGA

As the crystal structure (and the resulting distinct surface structure) of the support was theorized to play a mechanistic role in MSR,[9,24,25] the bulk structural features of the two selected Cu/ZrO_2 catalysts were assessed by synchrotron-based *in situ* X-ray diffraction and *operando* DTA/TG. The crystal structure of both the monoclinic and the tetragonal support materials are not altered by any of the applied treatments without any exception.

Exemplarily, the full set of diffractograms of one representative sample is shown in detail (CmZAc-imp7, Figure 5) with the rest being presented in the SI (Section G, Figures S12-S15). The information about the bulk phase(s) of Cu as a function of MSR reaction temperature is included in all catalytic MSR graphs as a color code.

The structural stability of m-ZrO_2 under the chosen MSR conditions as well as the expected temperature-induced expansion of the crystal lattice are clearly visible for CmZAc-imp7 in Figure 5. The Cu phase remains metallic over the course of the experiment, except for a small temperature region from 180 to 220 °C, where minor intermediary oxidation to Cu_2O (see magnified region) can be observed.

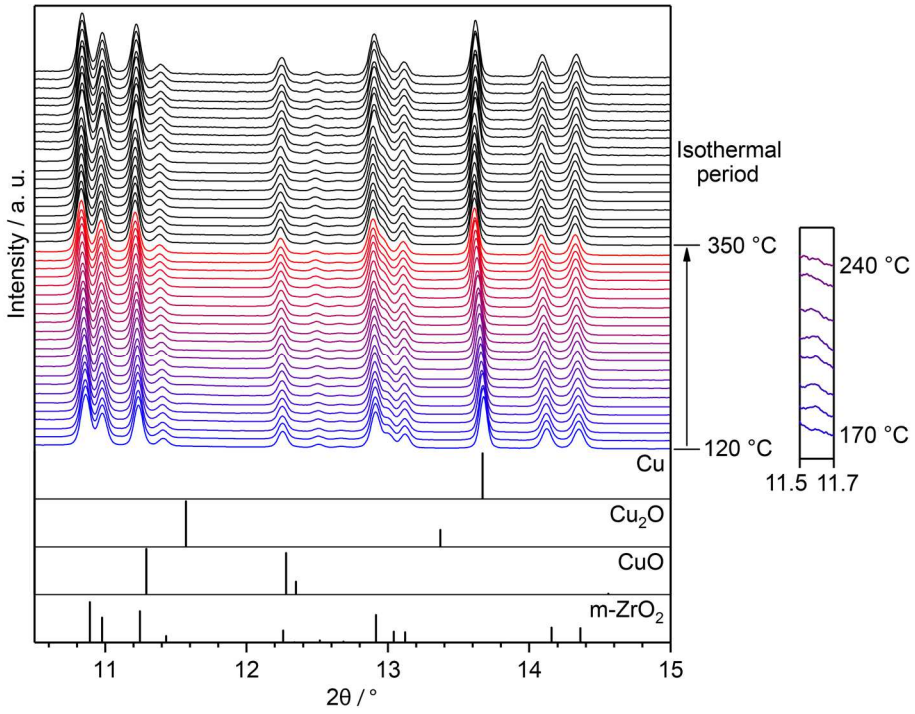

Figure 5: *In situ* XRD measurements of CmZAc-imp7 in the MSR mixture between 120 °C and 350 °C. The temperature evolution is color-coded with the heating period as a gradient from blue to red and the isothermal period in black. All reflections of m-ZrO_2, Cu, Cu_2O and CuO are marked at the bottom. The magnified region of the main reflection of Cu_2O on the right illustrates the intermediary formation of traces of this species. The references are taken from the ICDD database[53]: t-ZrO_2 (ICDD No. 00-050-1089)[15], m-ZrO_2 (calculated from the crystal structure by Yashima *et al.*[54] using VESTA 3[55]), cubic Cu (00-004-0836)[56], monoclinic CuO (00-045-0937)[57] and cubic Cu_2O (00-005-0667)[58].

To corroborate the redox trends of the Cu phases during the heating phase in MSR, *operando* DTA/TG was performed on the representative sample CmZAc-imp7 (Figure 6). No significant change of the mass can be observed during pre-oxidation, whereas pre-reduction causes a mass loss of 1.59 wt%, corresponding to a reduction of 1.82 mg CuO to 1.46 mg Cu. Upon introduction of the MSR mixture, a mass increase of 0.16 wt% indicates a slight oxidation, which may be interpreted as the oxidation of 0.29 mg Cu to 0.33 mg Cu_2O (1.43 wt% Cu_2O). Between the end of the heating phase and the beginning of the isothermal

period, a mass loss of roughly 0.05 wt% (equivalent to a reduction of 0.1 mg Cu_2O to Cu) is obtained, which suggests a partial reduction of the intermediately formed Cu_2O to Cu. The general trend of this evolution of copper oxidation states agrees with the results obtained by *in situ* XRD (*cf.* Figure 2 Panel A and Figure 5), since the amount of Cu_2O formation in MSR that is observed with TGA lies in the range of the detection limit of XRD and should therefore be barely (or not at all) visible.

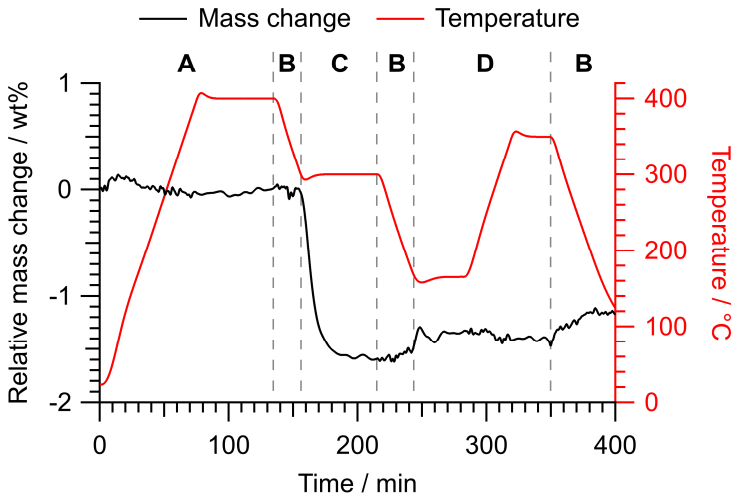

Figure 6: *Operando* DTA/TG measurements of CmZAc-imp7. The mass loss (black) and the temperature (red) are plotted *vs.* the measurement time. The bold letters denote the following compositions of the gas phase: **A** 20 vol% O_2 in He; **B** He; **C** 5 vol% H_2 in He; **D** 10 vol% MSR mixture in He. Sample mass: 23.06 mg.

3.3.3. Identification of crucial MSR reaction intermediates on Cu-ZrO_2 catalysts by in situ FT-IR spectroscopy and its consequences for the CO_2 selectivity

Figure 7 Panel A depicts the heating phase and the subsequent isothermal period in MSR on the CmZAc-imp7. In the course of the reaction, methanol is converted and CO_2, accompanied by small amounts of CO, is formed. The catalytic light-off temperatures are visible in Figure 7 Panel B, where the curves illustrate the temperature-dependent intensities of selected characteristic peaks of the different species. The assignment of the wavenumbers to the

respective components is compiled in Table 4. The light-off temperatures determined by FT-IR (180 °C for CO_2 and 240 °C for CO) match the corresponding values from the catalytic characterization with the recirculating batch reactor (165 °C for CO_2 and 240 °C for CO, see Table 5). The inset in Figure 7 Panel B emphasizes the evolution of the adsorbate species methoxy and formate as well as formaldehyde in the gas phase. This is also visualized in the form of three complete spectra at the start of MSR as well as the beginning and the end of the isothermal period in Figure S8 Panel A, revealing the formation of considerable amounts of gaseous formaldehyde, starting at the same temperature as CO_2, as well as the methoxy species. The visibility of formaldehyde implies that it reacts slowly on CmZAc-imp7 and is, thus, released into the gas phase. Because CmZAc-imp7 forms predominantly carbon dioxide, re-adsorption and further CO_2-selective oxidation of formaldehyde must occur at the phase boundary between Cu and m-ZrO_2, as the pure m-ZrO_2 support selectively catalyzes CO formation *via* formaldehyde dehydrogenation (see Figure 3). No build-up of adsorbed formates is visible in the course of the characterization, which means that these species react too fast to accumulate in significant amounts. This indicates that the binding strength of these formate species is suitable for rapid formaldehyde activation and conversion, *i.e.* not too weak (no formic acid in the gas phase) and not too strong (no long-lived formate species accumulate). The development of the methoxy population is similar to the formaldehyde profile, which is intrinsically related to the dehydrogenation of the methoxy species. *Vice versa*, the latter are formed from methanol by dissociative adsorption. The significant population of the intermediate methoxy species implies that their formation is fast and their further reaction rather slow, supporting literature reports that identify the dehydrogenation of methoxy species as the rate-determining step of MSR [2,59]. Mechanistically, the identification of formaldehyde supports the reaction pathway proposed by Takezawa *et al.* [60] and supported by Breen *et al.* [8], who found formaldehyde and formic acid as intermediates in MSR on Cu-based catalysts.

Following MSR, the gas phase was evacuated until the pressure stabilized. After an additional equilibration time of 5 min at 100 °C in the closed cell, the spectrum in Figure S8 Panel B in the SI reveals that all remaining physisorbed species desorb, resulting in the detection of traces of methanol and formaldehyde. This highlights our findings that all adsorbates on CmZAc-imp7 are bound weakly. In contrast, on CtZiPr-copr7 no signals of gas phase species are detected after equilibration in vacuum, but distinct signals of adsorbates remain visible in the spectra (*cf.* Figure 13 Panel B), which implies strongly bound species. Furthermore, we emphasize that no detectable amounts of carbonates or formates remain at the catalyst surface.

Table 4: Identification of species in the IR spectra.

Species	Mode	Frequency / cm^{-1}	References
$Methanol_{(g)}$	ν OH	3681	Shimanouchi[61]
	ν_{as} CH	3000+2960	
	ν_s CH	2844	
	overtone	2054	
	δ_{as} CH	1477	
	δ_s CH	1455	
	δ OH	1345	
	ρ CH_3	1060+1165	
	ν CO	1033	
$Methoxy_{(ads)}$	ν_{as} CH	2929	Frank *et al.*[2], Larmier *et al.*[62]
	ν_s CH	2818	
	ρ CH_3	1141	
	ν CO	1046	
$Formaldehyde_{(g)}$	ν CO (Q-branch)	1746	Nakanaga *et al.*[63]
	ν CH	2755	
$Formate_{(ads)}$	ν CH	2894	Frank *et al.*[2], Larmier *et al.*[62]
	ν_{as} OCO	1574	
	ν_s OCO	1363	
	δ OH	1357	
$CO_{(g)}$	ν CO (R-branch)	2171	Smith[64]
$CO_{2\ (g)}$	ν_{as} CO (R-branch)	2360	Shimanouchi[61]
	combinational vibrations $\nu_{as} + \nu_s$	3733, 3627, 3704, 3596	
$CH_{4\ (g)}$	ν CH (Q-branch)	3016	Shimanouchi[61]

Explanations: ν = stretching vibrations, δ = bending vibrations, ρ = rocking vibrations.

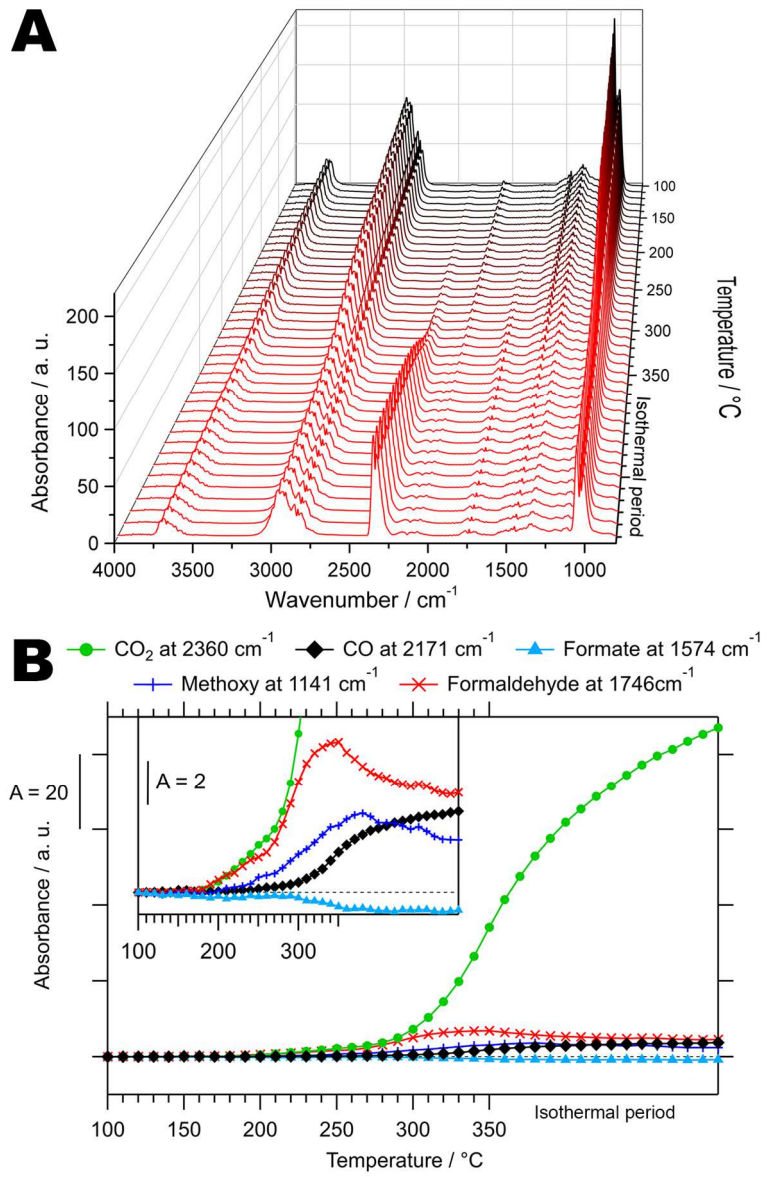

Figure 7: Panel A: *In situ* FT-IR spectra in the heating phase and the isothermal period of the MSR reaction on CmZAc-imp7 using the same experimental parameters as in the batch reactor. Panel B: Evolution of CO, CO_2 and several C_1 intermediates (methoxy, formaldehyde and formate; see inset) in the FT-IR reactor cell identified by selected wavenumbers (see legend) referenced to the initial spectrum at 100 °C. The absorbance was normalized to the total sample mass of 9.9 mg.

3.3.4. Correlated discussion of the influence of the ZrO_2 polymorph on the catalytic, structural and spectroscopic properties of Cu/ZrO_2 catalysts in MSR

In summary, the comparative discussion of the concerted results of bulk structure, catalytic and spectroscopic investigations of the influence of the ZrO_2 polymorph on the MSR performance of Cu-ZrO_2 catalysts already reveals considerable differences.

To improve the correlated discussion of results, those of the catalytic characterization of the systems obtained by corresponding copper isopropoxide impregnation of m- and t-ZrO_2 (CmZiPr-imp7 and CtZiPr-imp7; *cf.* Figures 8 and 9) are already discussed here. CmZiPr-imp7 displays a performance similar to (CmZAc-imp7), although the light-off temperatures of hydrogen and carbon dioxide are somewhat higher, resulting in a smaller region of 100% CO_2 selectivity. In comparison to CmZiPr-imp7, CtZiPr-imp7 exhibits the worst performance of all samples in terms of CO_2 selectivity (always around 20%), hydrogen and carbon dioxide light-off temperatures and activation energy (see Table 5). Additionally, a considerable amount of methane is formed, which is not observed for CmZiPr-imp7. This might be explained by a change of the reaction mechanism at the individual Cu phase boundary sites to the distinctly synthesized zirconia polymorphs as a result of their preparation-specific surface reactivity. t-ZrO_2 prepared in an analogous way has been shown to store hydrogen in a dissolved form in the surface region by X-ray photoelectron spectroscopy.[52,65] This hydrogen is considered to be highly reactive and can, thus, potentially lead to the formation of CH_4 from methanol or MSR intermediates. The amount of methane decreases slightly with increasing number of MSR cycles (see SI Figure S6), which could be linked to successive removal of sites capable of incorporating hydrogen.

CtZiPr-copr7 behaves very similar to CtZiPr-imp7 regarding the low CO_2 selectivity and the methane formation, but both effects are less pronounced. This potentially originates from the reduction of the effects stemming purely from the support, because Cu is able to partially block/modify these reactive sites during synthesis. The low CO_2 selectivity of the catalysts containing t-ZrO_2 might tentatively be explained by its additional support-located binding sites, as t-ZrO_2 exhibits both a high defectivity and a high degree of hydroxylation (see Köck

et al. [52]), featuring reactive Lewis acidic and Brønsted basic surface sites. We suggest a similar scenario as already reported in the literature, namely that strongly support-bonded formate species rather tend toward decarbonylation than toward decarboxylation (yielding CO instead of CO_2). [50–52,66] Additionally, CH_4 formation through reaction of "early" MSR intermediates (*i.e.* past methanol) with dissolved hydrogen in t-ZrO_2 appears to be superimposed. These observations prove that the preparation-specific chemical state of the zirconia support surface has a considerable impact on the overall catalyst performance in MSR. The extent to which the crystal structure itself, meaning the different intrinsic bulk electronic and structural properties of m- and t-ZrO_2, contributes to the individually observed catalytic properties seems to be much smaller compared to the modified chemical surface properties, which are determined and altered by the whole preparation history. In combination with the presented study, literature reports confirming the highly CO_2-selective performance of Cu/t-ZrO_2 systems in MSR[9,24] prove that both m-ZrO_2 and t-ZrO_2 can act as a support for a well-performing MSR catalyst.

No clear trend with respect to the evolution of the Cu oxidation state and the corresponding catalytic profile in MSR could be extracted upon comparing the differently prepared systems. CmZAc-imp7 stands out, exhibiting only slight intermediate oxidation to Cu_2O with the metallic phase being stable throughout the entire characterization (see Figure 5). All other samples, irrespective of the ZrO_2 polymorph, exhibit some oxidation to CuO, but are reduced once more during the isothermal phase (see SI Figures S12-S15). These findings suggest that the bulk phase of Cu is of minor importance for the catalytic properties, but rather the Cu surface/interface with chemically modified m-ZrO_2 or t-ZrO_2 surface/interface sites is responsible for the performance in MSR. A very similar evolution of the bulk Cu phase in contact with any ZrO_2 structure can obviously lead to remarkably different catalytic profiles (CmZiPr-imp7 and CtZiPr-imp7, see Figures 8 and 9, respectively).

3.4 Insights into the catalytic methanol steam reforming performance of Cu-ZrO_2 by using different synthesis routines and catalyst precursors: impregnation with Cu isopropoxide *vs.* Cu acetate and co-precipitation with Cu and Zr isopropoxide

It seems obvious that the synthesis routine influences the catalytic properties of a catalyst, whereby especially the surface area can be tuned by the choice of the calcination temperature. This is not straightforward if metastable components like t-ZrO_2 are present, which limits the gas-dependent calcination temperature to 400-450 °C to prevent transformation to the monoclinic modification. Moreover, the type of Cu as well as ZrO_2 precursors could have an impact on the chemical properties of the system by introducing basic or acidic surface sites, which will in turn modify the stability of selected reaction intermediates especially at the metal-oxide interface and, thus, potentially alter the reaction mechanism. In the following part, catalysts with the same support polymorph, but prepared by different synthesis routes, will be compared and the consequences discussed.

3.4.1 Methanol and formaldehyde steam reforming performance of Cu-ZrO_2 starting from differently synthesized Cu catalysts

The catalytic profile of CmZiPr-imp7 is depicted in Figure 8. It exhibits many characteristics of its Cu(II) acetate-impregnated counterpart of the identical support material (CmZAc-imp7, see Figure 2 Panel A). Among these are a temperature region, though narrower, with 100% CO_2 selectivity, suppressed formation of methane and a generally similar evolution of the reaction rates. In contrast, the initial catalytic cycle on this system exhibits excess CO_2 formation (or suppressed H_2 formation) with respect to the ideal MSR stoichiometry until shortly after the start of the isothermal phase, which is inferred from the deviating stoichiometry of the reaction not obeying the one of MSR as perfectly as the one of CmZAc-imp7. This effect diminishes with increasing number of catalytic cycles performed on the

same catalyst (see SI Figure S5), which can tentatively be explained by removal of carbonates as CO_2 and successive depopulation of binding sites for these species accompanying full catalyst reduction. Additionally, the formation rate of CO increases relative to the one of CO_2, thereby gradually lowering the CO_2 selectivity. Moreover, the evolution of the copper phases during MSR is much more complex in this system. Starting with metallic copper after pre-reduction, it is gradually oxidized until CuO is the predominant phase from approximately 270 °C to the beginning of the isothermal phase, where reduction sets in and only Cu^0 remains at the end of the measurement (see SI Figure S13). Since the evolution of copper is remarkably different in CmZAc-imp7 and CmZiPr-imp7, but the general characteristics of the catalytic profiles are similar, it can be concluded that the variable presence of bulk Cu species is not a key factor for the selectivities of the investigated zirconia-based catalysts in MSR.

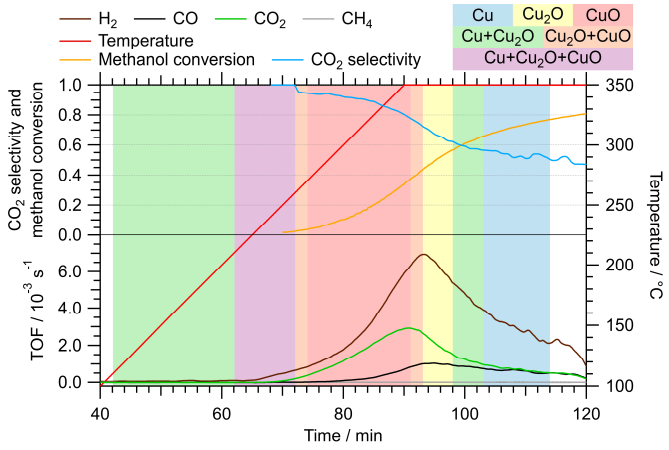

Figure 8: Methanol steam reforming profile of CmZiPr-imp7 between 100 °C and 350 °C. Color code: orange - methanol conversion, blue - CO_2 selectivity, formation rates of brown: H_2, black: CO, green: CO_2, gray: CH_4. The temperature regions of the involved bulk Cu phases as determined by *in situ* XRD (*cf.* Figure S13) are indicated by a colored background (see legend). Sample mass: 80.1 mg, heating rate: 5 °C min^{-1}.

The difference of the catalytic profiles caused by application of alternative impregnation routes is considerably more striking in the comparison of CtZiPr-imp7 (Figure 9) and its

acetate-impregnated equivalent (CtZAc-imp7, Figure 4). While the former displays substantial methane formation, even exceeding the production of CO_2, this effect is suppressed almost completely in the latter. However, the execution of repeated MSR cycles on CtZiPr-imp7 successively diminishes the formation of CH_4, decreasing the rate to a little more than half of its initial value (see SI Figure S6). As a concomitant effect, the CO_2 formation rate and the selectivity toward carbon dioxide increase alongside the decrease of methane production, which suggests that sites responsible for CH_4 formation are removed upon repeated catalytic cycling of this system. When t-ZrO_2 is present (also valid for the pure support), the MSR mixture including methanol adsorbs and desorbs upon heating, which renders the catalytic methanol conversion difficult to quantify, especially on CtZiPr-imp7 and CtZiPr-copr7. This is most pronounced in Figure 9 and 10, where the methanol conversion is still zero in regions where products are already being formed (and hence methanol already converted). The similarities of the two systems encompass the intermediate development of the Cu phase up to full oxidation, the generally low CO_2 selectivity and the non-stoichiometric hydrogen formation (with respect to ideal MSR).

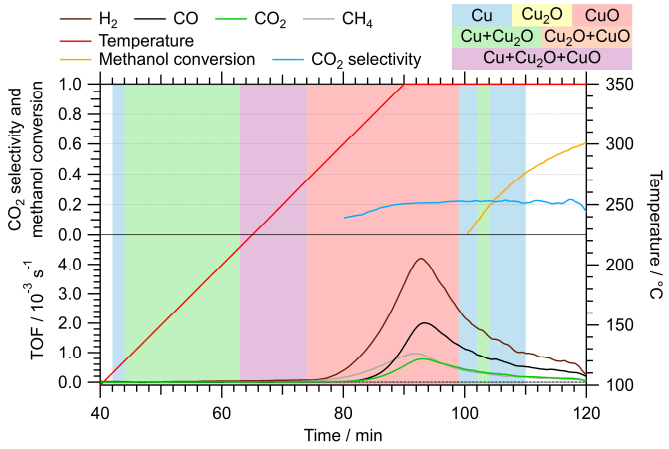

Figure 9: Methanol steam reforming profile of CtZiPr-imp7 between 100 °C and 350 °C. Color code: orange - methanol conversion, blue - CO_2 selectivity, formation rates of brown: H_2, black: CO, green: CO_2, gray: CH_4. The temperature regions of the involved bulk Cu phases, as determined by *in situ* XRD (*cf.* Figure S14), are indicated by a colored background

(see legend). Sample mass: 79.8 mg, heating rate: 5 °C min^{-1}. Methanol conversion for early reaction times unreliable due to reversible adsorption/desorption.

To relate the results of this work to an industrially relevant synthesis procedure, co-precipitation of Cu and Zr isopropoxide was employed (CtZiPr-copr7). The catalytic profile of this catalyst consisting of Cu and t-ZrO_2 is depicted in Figure 10 and exhibits many similar features compared to the other catalysts also containing t-ZrO_2 (CtZAc-imp7 and CtZiPr-imp7, see Figures 4 and 9). The most noteworthy differences are related to reduced methane formation as compared to CtZiPr-imp7, which might tentatively be explained by suppression of support-related surface-chemical effects due to partial blocking of reactive sites by Cu in the course of the synthesis, and a temperature region where metallic copper and CuO coexist without the presence of Cu_2O according to *in situ* XRD.

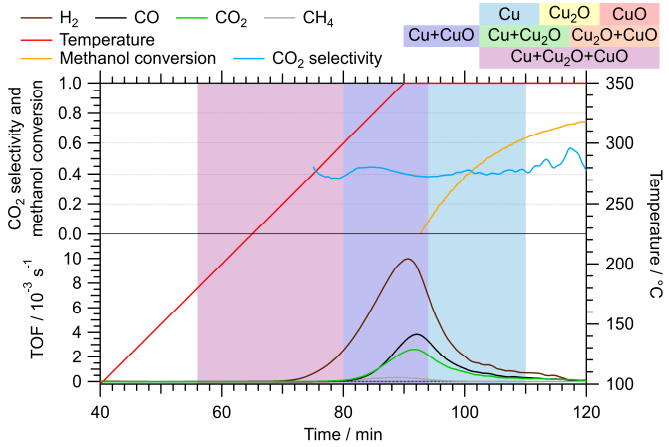

Figure 10: Methanol steam reforming profile of CtZiPr-copr7 between 100 °C and 350 °C. Color code: orange - methanol conversion, blue - CO_2 selectivity, formation rates of brown: H_2, black: CO, green: CO_2, gray: CH_4. The temperature regions of the involved bulk Cu phases, as determined by *in situ* XRD (*cf.* Figure S15), are indicated by a colored background (see legend). Sample mass: 67.1 mg, heating rate: 5 °C min^{-1}. Methanol conversion unreliable for early reaction times due to reversible adsorption/desorption.

Formaldehyde steam reforming (FSR) on pure t-ZrO_2 produces approximately 2.5 times more CO at the end of the isothermal period than H_2 and more methane than CO_2, which are both merely formed in traces. The onset temperatures of CO (≈ 250 °C) and H_2 (≈ 300 °C) are almost identical as on pure m-ZrO_2 (see Figure 3 Panel A), whereas the ratio of CO and hydrogen amounts to approximately 1.33 on m-ZrO_2. CtZiPr-copr7 shows a similar behavior as CmZAc-imp7 in FSR concerning the non-stoichiometric formation of CO_2, which can be explained tentatively by decomposition of surface-specific adsorbates formed *via* chemical bonding of the reactants at lower temperatures. The CO_2 selectivity of CtZiPr-copr7 in FSR stabilizes in the isothermal period, but at a slightly higher value (50% instead of 40%) than in MSR. Additionally, the methane formation is decreased in comparison with MSR. In contrast to the monoclinic zirconia-based systems presented in Figure 3, the total amount of CO produced by the pure tetragonal support is approximately half of the amount formed by CtZiPr-copr7. This implies that not only the support-located formation and/or spillover of formate species, but also the chemical nature of the Cu/t-ZrO_2 phase boundary and/or the state of Cu at the interface stabilized by the support leads to the poor CO_2 selectivity of this system in MSR. The apparent activation energy for CO_2 formation is considerably lower in FSR (≈ 84 kJ mol^{-1}) than in MSR (≈ 99 kJ mol^{-1}, both values were determined from the activity in µmol g_{Cu}^{-1} s^{-1} for better comparability), supporting the potential occurrence of formaldehyde as an intermediate in MSR.

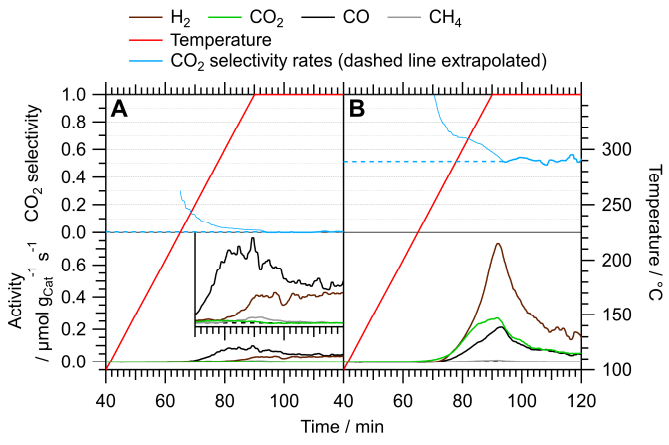

Figure 11: Panel A: Formaldehyde steam reforming profile on pure t-ZrO_2 (sample mass: 98.1 mg) including a zoomed in region of the formation rates. Panel B: Formaldehyde steam reforming profile on CtZiPr-copr7, sample mass: 27.5 mg) between 100 °C and 350 °C. Color code: blue - CO_2 selectivity, formation rates of brown: H_2, black: CO, green: CO_2, gray: CH_4. At low CO/CO_2 formation rates, the CO_2 selectivity cannot be quantified reliably. There, a dashed line represents the extrapolated reasonable value. The same extrapolation was performed for regions, where the selectivity pattern stabilizes after excess formation of one compound. Heating rate: 5 °C min^{-1}

3.4.2 Identification of crucial MSR reaction intermediates on Cu-ZrO_2 catalysts by in situ FT-IR spectroscopy and its consequences for CO_2 selectivity

As one representative sample containing t-ZrO_2, a co-precipitated Cu-ZrO_2 catalyst (CtZiPr-copr7) was characterized more thoroughly by *operando* DTA/TG and *in situ* FT-IR to infer further mechanistic details that help in understanding the catalytic MSR profile differences of Cu in contact with either m-ZrO_2 or t-ZrO_2. Additionally, an exemplary TEM characterization of CtZiPr-copr7 is given in the SI (see SI section F, Figures S10 and S11).

The *operando* DTA/TG measurement of CtZiPr-copr7 (Figure 12) illustrates a considerable mass loss upon pre-oxidation, which is linked to water that is released by removal of surface OH-groups and adsorbates. Since the tetragonal polymorph of zirconia is metastable, the calcination temperature and duration cannot be increased above certain values without inducing partial transformation to the monoclinic modification. ICP-OES delivers a Cu content of 4.4 wt% Cu in the calcined state and pre-reduction leads to an expected mass loss of 1.68 wt%. This value can be related to the reaction of 1.78 mg CuO to Cu, assuming that only the reduction of CuO accounts for the mass loss. However, this would imply a total copper content of 6.63 wt%. In the beginning of the catalytic phase (at 165 °C), the mass increases again by 1.45 wt% corresponding to an almost complete oxidation of the Cu phase

to CuO. In the course of the temperature ramp and the subsequent isothermal period, a mass loss of 1.63 wt% is observed, which can be explained by an almost complete re-reduction of CuO to metallic copper. These results agree with the *in situ* XRD data very well (*cf.* Figure 10 and Figure S15 in the SI).

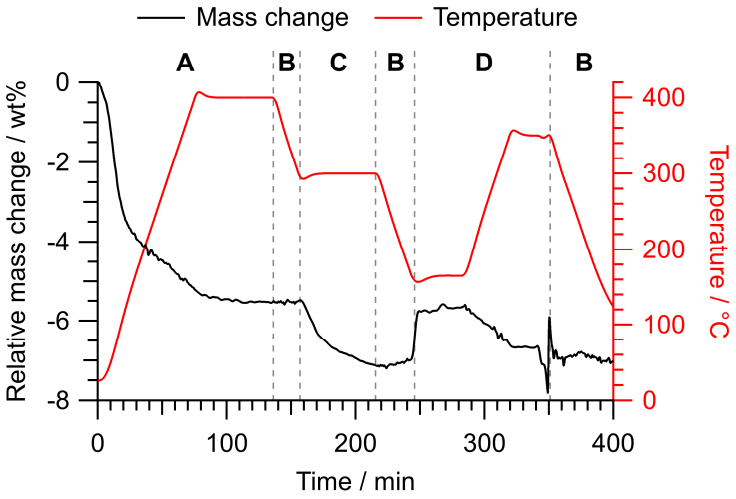

Figure 12: *Operando* DTA/TG measurements of CtZiPr-copr7. The mass loss (black) and the temperature (red) are plotted *vs.* the measurement time. The bold letters denote the following compositions of the gas phase: **A** 20 vol% O_2 in He; **B** pure He; **C** 5 vol% H_2 in He; **D** 10 vol% MSR mixture in He.

The *in situ* FT-IR measurements of MSR on CtZiPr-copr7 are highlighted in Figure 13 Panel A and reveal an almost complete conversion of methanol at the end of the isothermal period. Due to different initial MSR reactant pressures of the two measurements shown in Figure 7 and Figure 13, this cannot be directly related to the relative catalytic activities. The formation of CO_2 and CO is visible and the respective catalytic light-off temperatures can be found in Figure S9 Panel A in the SI. They show a slight shift to lower temperatures (around 250 °C for CO_2 and CO) in comparison to the values obtained with the recirculating batch reactor (about 280 °C for CO_2 and CO, see Table 5). The evolution of intermediates is highlighted in an inset in Figure S9 Panel A, which reveals much less formation of formaldehyde in the gas

phase as compared to CmZAc-imp7. Furthermore, the formaldehyde becomes fully consumed in the course of the isothermal period. Although formaldehyde conversion is fast in this system, considerable amounts of intermediate and/or spectator formate species can be observed on the catalyst, in contrast to CmZAc-imp7.

The binding strength of some of these formates is obviously rather large, as they survive after pump-down and the associated desorption of weakly bonded surface species (see Figure 13 Panel B). We, thus, suspect that some of them could be prone to decarbonylation yielding CO as a by-product and a surface hydroxyl group. The altered formate chemistry of the support could tentatively explain the much lower CO_2 selectivity of CtZiPr-copr7 compared to CmZAc-imp7, where the occurrence of temperature-stable formate species could not be observed. Slightly before the start of the isothermal period, the methoxy species that is present from the beginning (see black curve in Figure S9 Panel B) is converted, which takes place almost in parallel to the increase of CO. In contrast to CmZAc-imp7, where the methoxy species are only formed around 250 °C and not fully converted, the pronounced depletion of these intermediates, which are already present at the beginning of the characterization on CtZiPr-copr7, provides important mechanistic hints for enhanced CO formation and lack of CO_2 selectivity.

Differences in the stability and/or bonding type of methoxy species were previously related to different reaction pathways of CO hydrogenation on ZrO_2.[67] The site conversion of some bridged (b-)methoxy species to the terminal ones on ZrO_2 was directly observed by infrared spectroscopy between 250 and 350 °C, accompanied by thermal decomposition of co-adsorbed formate species. The observed adsorbate species could also be detected on ZrO_2 after exposure to a CO hydrogenation mixture at 250 °C. They identify b-methoxy species at 1043 cm^{-1} (ν(CO)), terminal (t-)methoxy species at 1145 cm^{-1} (ν(CO)) and formate species at 1369 cm^{-1} (δ(CH)) as well as 1568 cm^{-1} (ν_{as}(OCO)). The remaining adsorbates after equilibration in vacuum in Figure 13 Panel B agree very well with the literature values from

the study by Ouyang *et al.*[67], as bands at 1046, 1148, 1370 and 1585 cm^{-1} were observed on CtZiPr-copr7. Since these strikingly similar intermediates are observed in both studies, the high formation of CO on CtZiPr-copr7 can tentatively be interpreted as the reversed mechanism of CO hydrogenation on ZrO_2 presented by Ouyang *et al.*[67].

The aforementioned possible decarbonylation of strongly bound formates to CO and hydroxyl groups is confirmed in Figure 13 panel B by peaks at 3743 cm^{-1} (ν(OH) of terminal OH groups) and 3689 cm^{-1}, as well as 3649 cm^{-1} (ν(OH) of multi-coordinated OH groups).[52] In contrast to these peaks, the ν(OH) stretching modes of bicarbonates on an analogously synthesized t-ZrO_2 sample were observed around 3610 cm^{-1}, therefore clearly identifying the peaks on CtZiPr-copr7 as hydroxyl groups.[52]

Note that the molar attenuation coefficient ε of CO_2 is much higher compared to CO (the absorbance of the peak maximum of CO_2 at 2360 cm^{-1} is more than one order of magnitude higher than the peak maximum of CO at 2171 cm^{-1} at the same concentration in the gas phase, which was determined in reference spectra recorded with the pure gases). This is the reason for the apparently very CO_2-selective performance suggested by Figure S9 Panel A and, therefore, FT-IR is not suitable for the quantitative determination of the CO_2 selectivity.

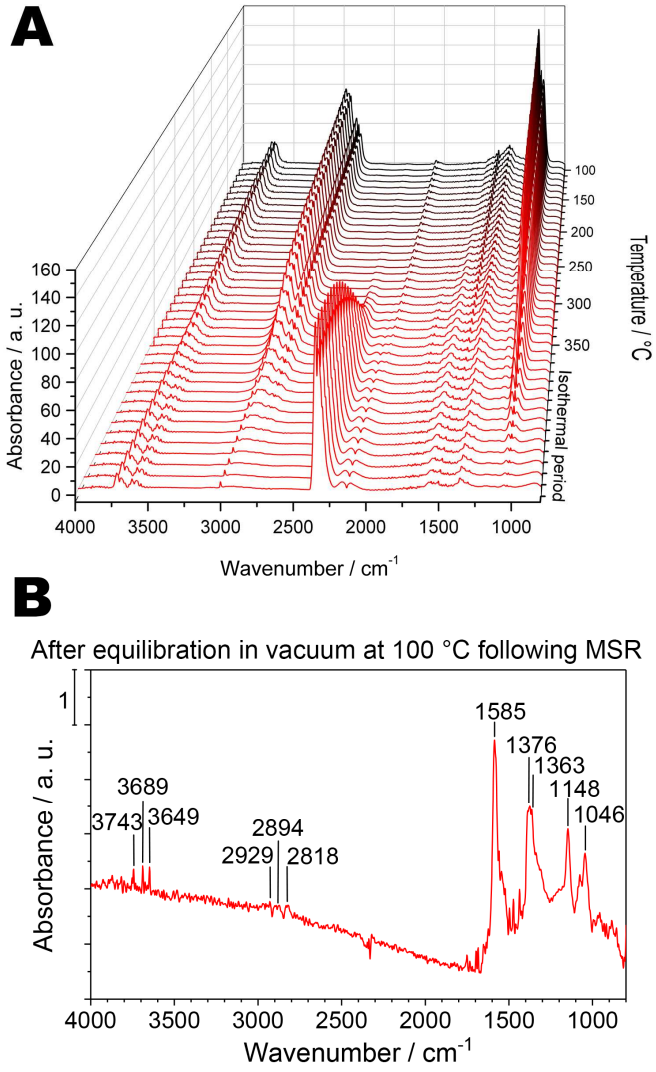

Figure 13: Panel A: *In situ* FT-IR spectra collected in the heating phase and the isothermal period on CtZiPr-copr7 during MSR using the same experimental parameters as in the recirculating batch reactor. Panel B: Representative spectrum at 100 °C after equilibration in vacuum following MSR. The absorbance was normalized to the total sample mass of 8.8 mg.

To verify the formation of methane in systems containing tetragonal zirconia during MSR, FT-IR spectra were recorded after complete conversion of methanol, which overlaps with the characteristic Q-branch of the rotational-vibrational spectrum of CH_4. This revealed the presence of traces of methane at the end of the isothermal period of MSR as well as in the beginning of vacuum desorption experiments (Figure 14 Panels A and B). These signals could not be observed in MSR with the Cu/m-ZrO_2 catalysts and are tentatively explained by the

presence of dissolved/adsorbed hydrogen in t-ZrO_2, facilitating the formation of CH_4 from MSR educts or intermediates. The formation of methane from a methanol steam reforming mixture mechanistically requires the promotion of C-O bond breaking followed by hydrogenation of CH_x intermediates, provided by the present t-ZrO_2 that has previously been shown to be capable of surface carbide formation with CO_2 and dissolution of H-atoms.[52,65] The methane formation mechanism may additionally be augmented by an active interface to Cu in this sample.

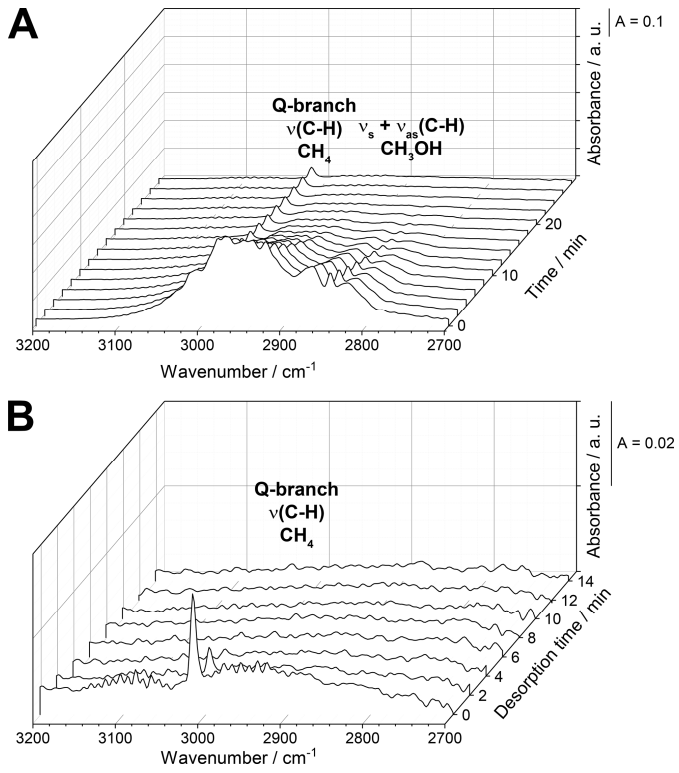

Figure 14: Methane gas phase signal on CtZiPr-copr7 visible at the end of the isothermal period in MSR (Panel A) and during vacuum desorption after catalysis (Panel B).[61,68,69]

3.4.3. Correlated discussion of the influence of the synthesis procedure on the catalytic, structural and spectroscopic properties of Cu/ZrO_2 catalysts in MSR

Compared to the impact of the support's surface structure including its potentially modified physico-chemical properties, the variation of the Cu precursor during impregnation influences the MSR performance to a much lower degree with the limitation of post-addition of the Cu

phase in this study, since impregnation as a two-step process was employed in all cases except for CtZiPr-copr7.

Speaking of the bulk Cu oxidation state, the *in situ* XRD investigations reveal an intermediate oxidation up to CuO in all systems except for CmZAc-imp7. The evolution of Cu during MSR is determined by the support polymorph and the respective surface properties. CmZAc-imp7 exhibits the most stable metallic Cu phase, whereas the other four systems show intermediate (bulk) oxidation to CuO. However, all catalysts are reduced again and display exclusively Cu^0 at the end of the isothermal phase. The high stability of the copper phase in CmZAc-imp7 can be explained by low Cu dispersion and, therefore, bulk-like Cu behavior, whereas t-ZrO_2 possesses a much higher surface area and a large number of defects – indicated by the ocher color of single phase ZrO_2[47] and reported in previous IR investigations[52] – and a high degree of hydroxylation, possibly resulting in enhanced redox kinetics of highly dispersed copper at the interface. Nevertheless, the bulk Cu oxidation state seems to play a minor role in MSR, as no clear connection to the CO_2 selectivity could be established, although the catalytic profiles display significantly different characteristics.

The influence of the synthesis procedure, *i.e.* impregnation *vs.* co-precipitation utilizing similar Cu precursors, on the catalytic properties seems to be limited to a subtle modification of the intrinsic chemical characteristics of the system stemming from the ZrO_2 polymorph itself and its specific synthesis history. The methane formation on catalysts containing t-ZrO_2 can be inhibited considerably by utilizing Cu acetate as the precursor instead of Cu isopropoxide, which causes considerable production of CH_4. This exclusiveness of methane formation in systems with tetragonal zirconia and Cu isopropoxide, which can also be observed, albeit to a considerably smaller extent, on pure t-ZrO_2, is an interesting phenomenon that should be investigated in more depth in the future. Moreover, the influence of dissolved hydrogen on methane formation from an MSR mixture in Cu-containing systems should be elucidated, since its presence has already been revealed in pure t-ZrO_2.[52]

A comparison with similar catalysts reported in literature is generally rather difficult, since the batch reactor setup predominantly utilized in this study is focused on the detection of trace byproducts. Therefore, it is especially suitable for the reliable determination of *e.g.* the CO_2 selectivity rather than the activity.

To put the activity in relation to MSR experiments performed in similar batch systems, Mayr *et al.* [27] provide maximum TOF(CO_2) values around 0.2 s^{-1} for inverse model catalysts of ZrO_2 on Cu at approximately 310 °C, where the corresponding value for CmZAc-imp7 amounts to 0.01 s^{-1}. However, here the partial pressure in the setup changes to a much lower degree due to the larger volume of the reactor and, therefore, the reaction equilibrium is influenced significantly less severely due to the successive formation of the MSR reaction products. Additionally, the number of active sites is estimated to be lower by a factor of 30-300 in [27] compared to this study, although even higher amounts of copper mass were used for the measurements. Lorenz *et al.* provide TOF(CO_2) values in MSR at 240 °C of 0.01 s^{-1} for 12% Pd on Ga_2O_3[70] and 0.0001 s^{-1} for 12% Pd on In_2O_3[71], where a value of 0.003 s^{-1} is obtained for CmZAc-imp7.

For copper-based catalysts, Takezawa *et al.*[60] report a TOF(H_2) of 0.037 $^{-1}$ at 220 °C for an impregnated Cu/SiO_2 catalyst in a flow reactor setup. A corresponding value of 0.0034 s^{-1} is observed for CmZAc-imp7 in the batch reactor. To put this into perspective, the thermodynamic and kinetic conditions in a batch reactor are different from a flow reactor, since fresh educts are continuously supplied and the products removed in the latter. If the Arrhenius fit for the TOF(H_2) of CmZAc-imp7 in the batch reactor is used for the extrapolation of the TOF, a value of 0.033 s^{-1} is obtained for 300 °C, in contrast to a maximum value of around 1 s^{-1} for the same catalyst in a flow reactor at the same temperature. This means that the values are difficult to compare directly, but assuming that this factor between batch and flow reactors is also roughly valid for 220 °C, CmZAc-imp7 would exhibit

a TOF(H_2) of approximately 0.1 s^{-1} in a flow reactor at this temperature, which compares well to the value of Takezawa *et al*[60] for Cu on SiO_2.

Szizybalski *et al.* [72] report values around 1-2 s^{-1} for H_2 formation on a Cu/t-ZrO_2 catalyst prepared by precipitation of zirconium propylate with tetramethylammonium hydroxide and addition of copper nitrate in a flow reactor setup at 250 °C. They also provide a value for an industrial Cu/ZnO/Al_2O_3 catalyst, which yields a value of approximately 0.08 s^{-1} at 250 °C. Employing the same assumption of a constant factor between batch and flow reactor characterization, a TOF(H_2) value of 0.3 s^{-1} can be estimated for CmZAc-imp7 at 250 °C, which is significantly higher than the industrial reference value, yet lower than the one for the Cu/t-ZrO_2 catalyst of Szizybalski *et al.* [72].

The most important parameters for the catalytic characterization of the samples 1 to 7 including the support materials in MSR are summarized in Table 5. The values for the apparent activation energy obtained by fitting the Arrhenius equation to the experimental formation rate of CO_2 are in the range of approximately 93-126 kJ mol^{-1}, which allows direct comparison with *e.g.* Zn-promoted Cu catalysts exhibiting values around 93 kJ mol^{-1}.[73]

Table 5: Summary of the most important catalytic parameters obtained on the five different Cu-containing catalysts and the pure supports.

Sample number	**6**	**1**	**3**	**7**	**2**	**4**	**5**
Acronym	**m**	**CmZAc-imp7**	**CmZiPr-imp7**	**t**	**CtZAc-imp7**	**CtZiPr-imp7**	**CtZiPr-copr7**
Nominal Cu loading (calcined) / wt%	-	6.9	6.9	-	6.9	6.9	6.9
Cu loading from ICP-OES (calcined) / wt%	-	6.7	9.7[a]	-	5.7[a]	7.3	4.4
BET surface area / m^2 g^{-1}	2	2	3	114	143	67	89
Light-off T(H_2) / °C	285	150	220	255	210	280	250
Light-off T(CO) / °C	290	240	260	285	270	300	280
Light-off T(CO_2) / °C	320	165	240	260	270	300	280
Light-off T(CH_4) / °C	315	-	-	260	-	260	240
Maximum CO_2 selectivity / %	11	100	100	49	50	23	57
T (100 %) / °C	-	165-240	240-260	-	-	-	-

Max. TOF CO_2	-	9.7	3.0	-	1.2	0.78	2.6
/ 10^{-3} s^{-1}		310 °C	350 °C		345 °C	350 °C	350 °C
TOF CO_2 at 250 °C	-	4.0	0.085	-	0.0071	0	0
/ 10^{-3} s^{-1}							
Max. TOF H_2	-	26	7.2	-	5.1	4.2	10
/ 10^{-3} s^{-1}		310 °C	350 °C		325 °C	350 °C	350 °C
TOF H_2 at 250 °C	-	10	0.50	-	0.53	0	0.021
/ 10^{-3} s^{-1}							
E_a / kJ mol^{-1}	-[b]	93	109	-[b]	119	126	121

Explanations: E_a = apparent activation energy obtained by fitting the Arrhenius equation to the experimental data of CO_2 in MSR; [a]value determined *via* oxidation-reduction-oxidation DTA-TG measurements; [b]determination impossible, because too little CO_2 is formed for a reliable fit.

4. Conclusions

In conclusion, by the chosen approach using different ZrO_2 polymorphs, catalyst precursors and synthesis routines, ZrO_2 is identified to exhibit a considerable versatility as support material and can be tuned in many ways to modify the catalytic properties of copper-containing catalysts in MSR.

To summarize the most important features, we note the following:

- Given the structural complexity of the Zr-O system (multiplied if present in a Cu-ZrO_2 interface) and its catalytic properties in MSR, deduction of general statements from selected and individual examples is extremely difficult.
- Bulk (crystal structure, particle size) and surface properties (acidic, basic, oxidative, reductive) of ZrO_2 alone can be beneficially or detrimentally modified by its preparation in many ways allowing to switch a Cu/ZrO_2 system between a CO_2-selective and an unselective state in MSR with the support in *both* the monoclinic or the tetragonal polymorph.
- The *support surface properties,* as a consequence of a specific synthesis routine, are found to be *the* steering parameter for high CO_2 selectivity exceeding the impact of the type of Cu precursor, the support bulk structure or the Cu bulk oxidation state. The studied catalysts containing either monoclinic or tetragonal ZrO_2 have certain characteristics in common: The former display 100% CO_2 selectivity in a certain

temperature region, whereas the latter are generally less CO_2-selective. These effects are tentatively explained by altered binding sites on the significantly more defective and more hydroxylated t-ZrO_2, invoking different binding and interfacial sites for water as well as C_1 intermediates. These features promote decarbonylation and potentially C-O bond breaking, which yields CO and CH_4, respectively.

- The comparison of representative catalysts including their pure support materials in FSR and MSR yields crucial insights into the capability of methanol activation and the CO_2 selectivity starting from methanol or formaldehyde. The amount of CO that is formed on the pure supports in relation to the amount of by-products produced by the respective catalyst containing Cu reveals crucial differences between systems with m-ZrO_2 and t-ZrO_2. The CO formation of Cu/m-ZrO_2 can be fully ascribed to a spillover of formate to the support, whereas Cu/t-ZrO_2 exhibits a CO-forming Cu-ZrO_2 interface in addition to a potential spillover of formaldehyde.

In view of providing a recipe for the technological development of a CO_2-selective Cu/ZrO_2 catalyst, we conclude with an array of detrimental properties that need to be avoided accordingly:

- t-ZrO_2 synthesized by precursors yielding a large number of Lewis acidic or Brønsted basic sites (such as Zr isopropoxide) is intrinsically too reactive, leading to undesired side reactions by stabilization of strongly bound formate and reactive methoxy species prone to decarbonylation (with and without copper).
- Cu/m-ZrO_2 does not stabilize these species, but its lack in CO_2 selectivity at higher temperatures can be explained *via* spillover of formaldehyde species to the support, as pure m-ZrO_2 mainly yields CO *via* formaldehyde decomposition in FSR.
- The support's defect chemistry and degree of hydroxylation, chemical parameters that depend on the complete preparation history of the specific zirconia sample, rather than its bulk structure, need to be controlled carefully, but eventually allow to balance the

binding strength of specific intermediates leading to CO_2 formation rather than CO production.

Supporting Information: Section A: Details of preparation of the catalysts; Section B: Detailed experimental; Section C: Catalytic characterization of the pure supports; Section D: Multiple MSR cycles on the Cu/ZrO_2 catalysts; Section E: Detailed *in situ* FT-IR analysis; Section F: *Ex situ* electron microscopy characterization; Section G: Additional *in situ* XRD patterns.

5. Acknowledgments

The work was financially supported by the Austrian Science Foundation (FWF) under SFB projects F4503-N16 and F4501-N16 and the DACH project I2877-N34. Further support was provided by the framework of the platform Materials- and Nanoscience and the special PhD program "Reactivity and Catalysis" at the University of Innsbruck. The authors additionally thank the Deutsche Forschungsgemeinschaft (DFG) for funding L. Zhang and the investigations at the Technische Universität Chemnitz (project AR 617/12-1). L. Schlicker appreciates the ALS for supporting his work with a doctoral fellowship. Financial support by the DFG within the framework of the German Initiative for Excellence is gratefully acknowledged. The authors further thank the Advanced Light Source (which is supported by the Director, Office of Science, Office of Basic Energy Sciences, of the U.S. Department of Energy under Contract No. DE-AC02-05CH11231), where *in situ* powder XRD measurements were conducted at the beamline 12.2.2 in the framework of the AP program ALS-08865. S. Vanicek acknowledges the project J-4158 granted by the FWF for financial support. We particularly thank the group of H. Huppertz from the Department of General, Inorganic and Theoretical Chemistry of the University of Innsbruck for providing the possibility of using their X-ray diffractometer for *ex situ* powder XRD measurements.

6. References

[1] K.A. Ali, A.Z. Abdullah, A.R. Mohamed, Recent development in catalytic technologies for methanol synthesis from renewable sources: A critical review, Renewable Sustainable Energy Rev. 44 (2015) 508–518.

[2] B. Frank, F. Jentoft, H. Soerijanto, J. Kröhnert, R. Schlögl, R. Schomäcker, Steam reforming of methanol over copper-containing catalysts: Influence of support material on microkinetics, J. Catal. 246 (2007) 177–192.

[3] Z. Baysal, S. Kureti, CO_2 methanation on Mg-promoted Fe catalysts, Appl. Catal., B 262 (2020) 118300.

[4] M. Behrens, M. Armbrüster, Methanol Steam Reforming, in: L. Guczi, A. Erdôhelyi (Eds.), Catalysis for Alternative Energy Generation, Springer New York, New York, NY, 2012, pp. 175–235.

[5] S. Velu, K. Suzuki, C.S. Gopinath, H. Yoshida, T. Hattori, XPS, XANES and EXAFS investigations of $CuO/ZnO/Al_2O_3/ZrO_2$ mixed oxide catalysts, Phys. Chem. Chem. Phys. 4 (2002) 1990–1999.

[6] S. Velu, K. Suzuki, M.P. Kapoor, F. Ohashi, T. Osaki, Selective production of hydrogen for fuel cells via oxidative steam reforming of methanol over CuZnAl(Zr)-oxide catalysts, Appl. Catal., A 213 (2001) 47–63.

[7] G.-S. Wu, D.-S. Mao, G.-Z. Lu, Y. Cao, K.-N. Fan, The Role of the Promoters in Cu Based Catalysts for Methanol Steam Reforming, Catal. Lett. 130 (2009) 177–184.

[8] J.P. Breen, J.R.H. Ross, Methanol reforming for fuel-cell applications: Development of zirconia-containing Cu-Zn-Al catalysts, Catal. Today 51 (1999) 521–533.

[9] H. Purnama, F. Girgsdies, T. Ressler, J.H. Schattka, R.A. Caruso, R. Schomäcker, R. Schlögl, Activity and Selectivity of a Nanostructured CuO/ZrO_2 Catalyst in the Steam Reforming of Methanol, Catal. Lett. 94 (2004) 61–68.

[10] M. Friedrich, S. Penner, M. Heggen, M. Armbrüster, High CO_2 selectivity in methanol steam reforming through ZnPd/ZnO teamwork, Angew. Chem. Int. Ed. 52 (2013) 4389–4392.

[11] R.J. Ackermann, S.P. Garg, E.G. Rauh, High-Temperature Phase Diagram for the System Zr-O, J. Am. Ceram. Soc. 60 (1977) 341–345.

[12] J.P. Abriata, J. Garcés, R. Versaci, The O–Zr (Oxygen-Zirconium) system, Bull. Alloy Phase Diagr. 7 (1986) 116–124.

[13] V.P. Oleshko, J.M. Howe, S. Shukla, S. Seal, High-Resolution and Analytical TEM Investigation of Metastable-Tetragonal Phase Stabilization in Undoped Nanocrystalline Zirconia, J. Nanosci. Nanotech. 4 (2004) 867–875.

[14] H.F. McMurdie, M.C. Morris, E.H. Evans, B. Paretzkin, W. Wong-NG, C.R. Hubbard, Methods of Producing Standard X-Ray Diffraction Powder Patterns, Powder Diffr. 1 (1986) 40–43.

[15] J. Málek, L. Beneš, T. Mitsuhashi, Powder diffraction data and Rietveld refinement of metastable t-ZrO_2 at low temperature, Powder Diffr. 12 (1997) 96–98.

[16] U. Martin, H. Boysen, F. Frey, Neutron powder investigation of tetragonal and cubic stabilized zirconia, TZP and CSZ, at temperatures up to 1400 K, Acta Crystallogr., Sec. B: Struct. Sci. 49 (1993) 403–413.

[17] P. Aldebert, J.-P. Traverse, Structure and Ionic Mobility of Zirconia at High Temperature, J. Am. Ceram. Soc. 68 (1985) 34–40.

[18] M. Kogler, E.-M. Köck, S. Vanicek, D. Schmidmair, T. Götsch, M. Stöger-Pollach, C. Hejny, B. Klötzer, S. Penner, Enhanced kinetic stability of pure and Y-doped tetragonal ZrO_2, Inorg. Chem. 53 (2014) 13247–13257.

[19] T. Chraska, A.H. King, C.C. Berndt, On the size-dependent phase transformation in nanoparticulate zirconia, Mater. Sci. Eng., A 286 (2000) 169–178.

[20] K. Li, J.G. Chen, CO_2 Hydrogenation to Methanol over ZrO_2-Containing Catalysts: Insights into ZrO_2 Induced Synergy, ACS Catal. 9 (2019) 7840–7861.

[21] S. Tada, A. Katagiri, K. Kiyota, T. Honma, H. Kamei, A. Nariyuki, S. Uchida, S. Satokawa, Cu Species Incorporated into Amorphous ZrO_2 with High Activity and Selectivity in CO_2-to-Methanol Hydrogenation, J. Phys. Chem. C 122 (2018) 5430–5442.

[22] S. Tada, S. Kayamori, T. Honma, H. Kamei, A. Nariyuki, K. Kon, T. Toyao, K.-i. Shimizu, S. Satokawa, Design of Interfacial Sites between Cu and Amorphous ZrO_2 Dedicated to CO_2-to-Methanol Hydrogenation, ACS Catal. 8 (2018) 7809–7819.

[23] H. Oguchi, H. Kanai, K. Utani, Y. Matsumura, S. Imamura, Cu_2O as active species in the steam reforming of methanol by CuO/ZrO_2 catalysts, Appl. Catal., A 293 (2005) 64–70.

[24] L. Mayr, B. Klötzer, D. Schmidmair, N. Köpfle, J. Bernardi, S. Schwarz, M. Armbrüster, S. Penner, Boosting Hydrogen Production from Methanol and Water by in situ Activation of Bimetallic Cu–Zr Species, ChemCatChem 8 (2016) 1778–1781.

[25] L. Mayr, N. Köpfle, B. Klötzer, T. Götsch, J. Bernardi, S. Schwarz, T. Keilhauer, M. Armbrüster, S. Penner, Microstructural and Chemical Evolution and Analysis of a Self-Activating CO_2-Selective Cu–Zr Bimetallic Methanol Steam Reforming Catalyst, J. Phys. Chem. C 120 (2016) 25395–25404.

[26] L. Mayr, B. Klötzer, D. Zemlyanov, S. Penner, Steering of methanol reforming selectivity by zirconia–copper interaction, J. Catal. 321 (2015) 123–132.

[27] L. Mayr, X. Shi, N. Köpfle, B. Klötzer, D. Zemlyanov, S. Penner, Tuning of the copper–zirconia phase boundary for selectivity control of methanol conversion, J. Catal. 339 (2016) 111–122.

[28] M. Inoue, H. Kominami, T. Inui, Novel synthesis method for thermally stable monoclinic zirconia: Hydrolysis of zirconium alkoxides at high temperatures with a

limited amount of water dissolved in inert organic solvent from the gas phase, Appl. Catal., A 121 (1995) L1-L6.

[29] K. Takahashi, H. Kobayashi, N. Takezawa, On the difference in reaction pathways of steam reforming of methanol over copper-silica and platinum-silica catalysts, Chem. Lett. 14 (1985) 759–762.

[30] V.I. Bukhtiyarov, I.P. Prosvirin, E.P. Tikhomirov, V.V. Kaichev, A.M. Sorokin, V.V. Evstigneev, *In situ* study of selective oxidation of methanol to formaldehyde over copper, React. Kinet. Catal. Lett. 79 (2003) 181–188.

[31] A. Knop-Gericke, M. Hävecker, T. Schedel-Niedrig, R. Schlögl, Characterisation of active phases of a copper catalyst for methanol oxidation under reaction conditions: an *in situ* X-ray absorption spectroscopy study in the soft energy range, Top. Catal. 15 (2001) 27–34.

[32] Z.-T. Wang, Y. Xu, M. El-Soda, F.R. Lucci, R.J. Madix, C.M. Friend, E.C.H. Sykes, Surface Structure Dependence of the Dry Dehydrogenation of Alcohols on Cu(111) and Cu(110), J. Phys. Chem. C 121 (2017) 12800–12806.

[33] M. Bowker, Active sites in methanol oxidation on Cu(110) determined by STM and molecular beam measurements, Top. Catal. 3 (1996) 461–468.

[34] N. Gerrits, G.-J. Kroes, An AIMD study of dissociative chemisorption of methanol on Cu(111) with implications for formaldehyde formation, J. Chem. Phys. 150 (2019) 24706.

[35] S. Sá, H. Silva, L. Brandão, J.M. Sousa, A. Mendes, Catalysts for methanol steam reforming—A review, Appl. Catal., B 99 (2010) 43–57.

[36] J.W. Evans, M.S. Wainwright, A.J. Bridgewater, D.J. Young, On the determination of copper surface area by reaction with nitrous oxide, Appl. Catal. 7 (1983) 75–83.

[37] L. Mayr, H. Lorenz, M. Armbrüster, S.A. Villaseca, Y. Luo, R. Cardoso, U. Burkhardt, D. Zemlyanov, M. Haevecker, R. Blume, A. Knop-Gericke, B. Klötzer, S. Penner, The

catalytic properties of thin film Pd-rich $GaPd_2$ in methanol steam reforming, J. Catal. 309 (2014) 231–240.

[38] C. Prescher, V.B. Prakapenka, DIOPTAS a program for reduction of two-dimensional X-ray diffraction data and data exploration, High Pressure Res. 35 (2015) 223–230.

[39] A. Doran, L. Schlicker, C.M. Beavers, S. Bhat, M.F. Bekheet, A. Gurlo, Compact low power infrared tube furnace for *in situ* X-ray powder diffraction, Rev. Sci. Instrum. 88 (2017) 13903.

[40] L. Schlicker, A. Doran, P. Schneppmüller, A. Gili, M. Czasny, S. Penner, A. Gurlo, Transmission *in situ* and *operando* high temperature X-ray powder diffraction in variable gaseous environments, Rev. Sci. Instrum. 89 (2018) 33904.

[41] E.-M. Köck, M. Kogler, R. Pramsoler, B. Klötzer, S. Penner, A high-temperature, ambient-pressure ultra-dry operando reactor cell for Fourier-transform infrared spectroscopy, Rev. Sci. Instrum. 85 (2014) 84102.

[42] E.S. Vasiliadou, T.M. Eggenhuisen, P. Munnik, P.E. de Jongh, K.P. de Jong, A.A. Lemonidou, Synthesis and performance of highly dispersed Cu/SiO_2 catalysts for the hydrogenolysis of glycerol, Appl. Catal., B 145 (2014) 108–119.

[43] S. Natesakhawat, J.W. Lekse, J.P. Baltrus, P.R. Ohodnicki, B.H. Howard, X. Deng, C. Matranga, Active Sites and Structure–Activity Relationships of Copper-Based Catalysts for Carbon Dioxide Hydrogenation to Methanol, ACS Catal. 2 (2012) 1667–1676.

[44] CasaXPS: Processing Software for XPS, AES, SIMS and More, Casa Software Ltd.

[45] W.H. Gries, A Universal Predictive Equation for the Inelastic Mean Free Pathlengths of X-ray Photoelectrons and Auger Electrons, Surf. Interface Anal. 24 (1996) 38–50.

[46] M.C. Biesinger, Advanced analysis of copper X-ray photoelectron spectra, Surf. Interface Anal. 49 (2017) 1325–1334.

[47] U. Anselmi-Tamburini, J.N. Woolman, Z.A. Munir, Transparent Nanometric Cubic and Tetragonal Zirconia Obtained by High-Pressure Pulsed Electric Current Sintering, Adv. Funct. Mater. 17 (2007) 3267–3273.

[48] B. Savoini, C. Ballesteros, J.E. Muñoz Santiuste, R. González, Y. Chen, Thermochemical reduction of yttria-stabilized-zirconia crystals: Optical and electron microscopy, Phys. Rev. B 57 (1998) 13439–13447.

[49] H. Zhang, Z. Li, B.-N. Kim, K. Morita, H. Yoshida, K. Hiraga, Y. Sakka, Highly Infrared Transparent Nanometric Tetragonal Zirconia Prepared by High-Pressure Spark Plasma Sintering, J. Am. Ceram. Soc. 94 (2011) 2739–2741.

[50] E.-M. Köck, M. Kogler, T. Bielz, B. Klötzer, S. Penner, In Situ FT-IR Spectroscopic Study of CO_2 and CO Adsorption on Y_2O_3, ZrO_2, and Yttria-Stabilized ZrO_2, J. Phys. Chem. C 117 (2013) 17666–17673.

[51] E.-M. Köck, M. Kogler, B. Klötzer, M.F. Noisternig, S. Penner, Structural and Electrochemical Properties of Physisorbed and Chemisorbed Water Layers on the Ceramic Oxides Y_2O_3, YSZ, and ZrO_2, ACS Appl. Mater. Interfaces 8 (2016) 16428–16443.

[52] E.-M. Köck, M. Kogler, T. Götsch, L. Schlicker, M.F. Bekheet, A. Doran, A. Gurlo, B. Klötzer, B. Petermüller, D. Schildhammer, N. Yigit, S. Penner, Surface chemistry of pure tetragonal ZrO_2 and gas-phase dependence of the tetragonal-to-monoclinic ZrO_2 transformation, Dalton Trans. 46 (2017) 4554–4570.

[53] ICDD Database PDF-4+, International Centre for Diffraction Data, Newtown Square, PA 19073, USA, 2010.

[54] M. Yashima, T. Hirose, S. Katano, Y. Suzuki, M. Kakihana, M. Yoshimura, Structural changes of ZrO_2-CeO_2 solid solutions around the monoclinic-tetragonal phase boundary, Phys. Rev. B 51 (1995) 8018–8025.

[55] K. Momma, F. Izumi, *VESTA 3* for three-dimensional visualization of crystal, volumetric and morphology data, J. Appl. Cryst. (Journal of Applied Crystallography) 44 (2011) 1272–1276.

[56] H.E. Swanson, E. Tatge, Standard X-ray diffraction patterns, Natl. Bur. Stand.(US) Circ. 539 1 (1953) 15.

[57] N.E. Brese, M. O'Keeffe, B.L. Ramakrishna, R.B. von Dreele, Low-temperature structures of CuO and AgO and their relationships to those of MgO and PdO, J. Solid State Chem. 89 (1990) 184–190.

[58] R. Restori, D. Schwarzenbach, Charge density in cuprite, Cu_2O, Acta Crystallogr., Sec. B: Struct. Sci. 42 (1986) 201–208.

[59] B.A. Peppley, J.C. Amphlett, L.M. Kearns, R.F. Mann, Methanol–steam reforming on $Cu/ZnO/Al_2O_3$ catalysts. Part 2. A comprehensive kinetic model, Appl. Catal., A 179 (1999) 31–49.

[60] N. Takezawa, N. Iwasa, Steam reforming and dehydrogenation of methanol: Difference in the catalytic functions of copper and group VIII metals, Catal. Today 36 (1997) 45–56.

[61] T. Shimanouchi, Tables of Molecular Vibrational Frequencies Consolidated Part 5, J. Phys. Chem. Ref. Data 1 (1972) 1–160.

[62] K. Larmier, W.-C. Liao, S. Tada, E. Lam, R. Verel, A. Bansode, A. Urakawa, A. Comas-Vives, C. Copéret, CO_2-to-Methanol Hydrogenation on Zirconia-Supported Copper Nanoparticles: Reaction Intermediates and the Role of the Metal-Support Interface, Angew. Chem. Int. Ed. 56 (2017) 2318–2323.

[63] T. Nakanaga, S. Kondo, S. Saëki, Infrared band intensities of formaldehyde and formaldehyde - d_2, J. Chem. Phys. 76 (1982) 3860–3865.

[64] A.L. Smith, The Coblentz Society Desk Book of Infrared Spectra, in: C.D. Carver (Ed.), The Coblentz Society Desk Book of Infrared Spectra, The Coblentz Society, Kirkwood, MO, 1982.

[65] M. Youssef, B. Yildiz, Hydrogen defects in tetragonal ZrO_2 studied using density functional theory, Phys. Chem. Chem. Phys. 16 (2014) 1354–1365.

[66] M.A. Henderson, Complexity in the Decomposition of Formic Acid on the TiO_2(110) Surface, J. Phys. Chem. B 101 (1997) 221–229.

[67] F. Ouyang, J.N. Kondo, K.-i. Maruya, K. Domen, Site Conversion of Methoxy Species on ZrO_2, J. Phys. Chem. B 101 (1997) 4867–4869.

[68] F. Le Peltier, P. Chaumette, J. Saussey, M.M. Bettahar, J.C. Lavalley, *In situ* FT-IR and kinetic study of methanol synthesis from CO_2/H_2 over $ZnAl_2O_4$ and Cu–$ZnAl_2O_4$ catalysts, J. Mol. Catal. A: Chem. 132 (1998) 91–100.

[69] M. Kogler, E.-M. Köck, B. Klötzer, S. Penner, Structure–Property Relationships in the Y_2O_3–ZrO_2 Phase Diagram: Influence of the Y-Content on Reactivity in C1 Gases, Surface Conduction, and Surface Chemistry, J. Phys. Chem. C 120 (2016) 22443–22454.

[70] H. Lorenz, S. Penner, W. Jochum, C. Rameshan, B. Klötzer, Pd/Ga_2O_3 methanol steam reforming catalysts: Part II. Catalytic selectivity, Appl. Catal., A 358 (2009) 203–210.

[71] H. Lorenz, S. Turner, O.I. Lebedev, G. van Tendeloo, B. Klötzer, C. Rameshan, K. Pfaller, S. Penner, Pd–In_2O_3 interaction due to reduction in hydrogen: Consequences for methanol steam reforming, Appl. Catal., A 374 (2010) 180–188.

[72] A. Szizybalski, F. Girgsdies, A. Rabis, Y. Wang, M. Niederberger, T. Ressler, In situ investigations of structure–activity relationships of a Cu/ZrO_2 catalyst for the steam reforming of methanol, J. Catal. 233 (2005) 297–307.

[73] C. Rameshan, W. Stadlmayr, S. Penner, H. Lorenz, N. Memmel, M. Hävecker, R. Blume, D. Teschner, T. Rocha, D. Zemlyanov, A. Knop-Gericke, R. Schlögl, B. Klötzer,

Hydrogen production by methanol steam reforming on copper boosted by zinc-assisted water activation, Angew. Chem. Int. Ed. 51 (2012) 3002–3006.

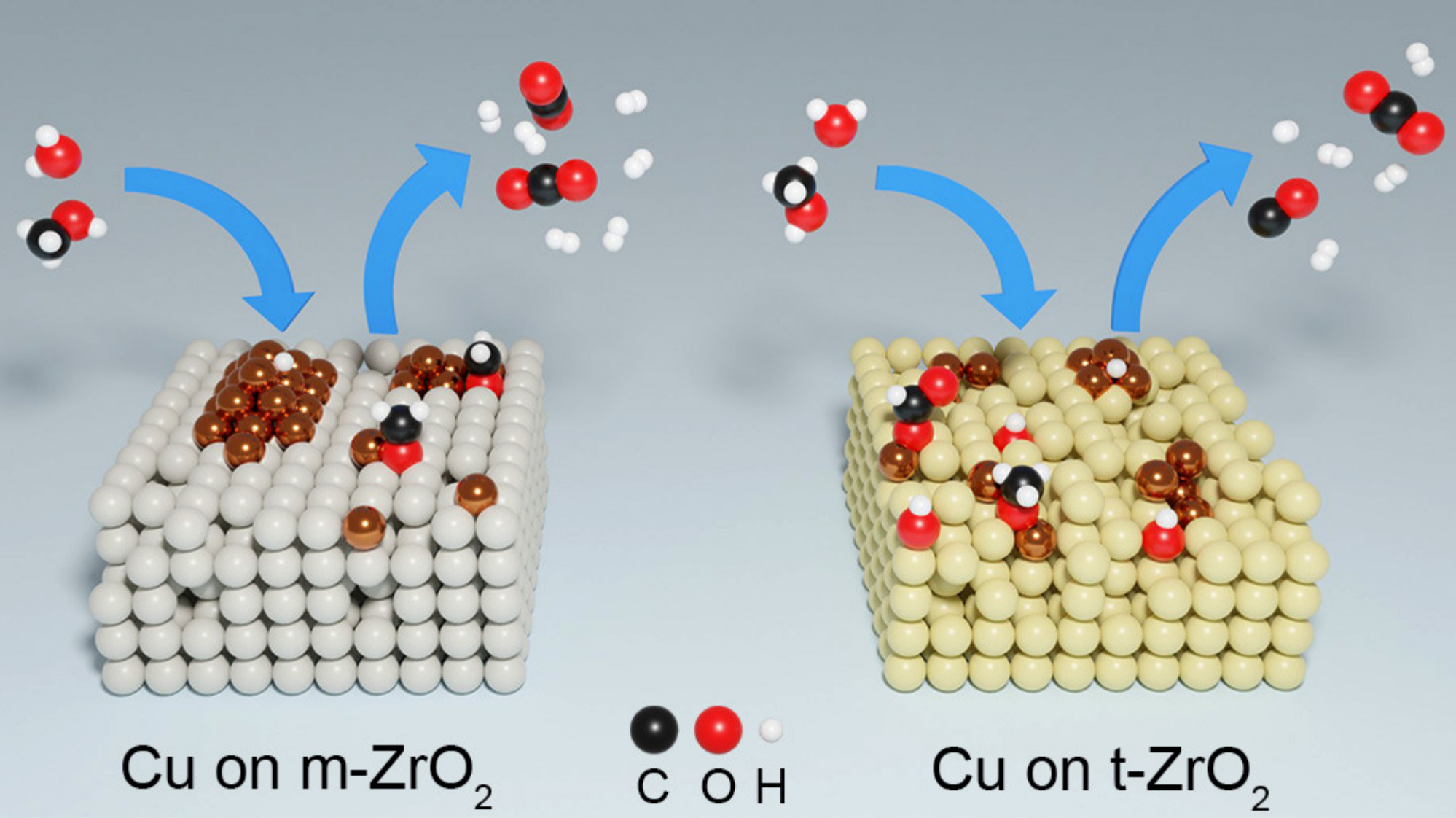
Cu on m-ZrO2
C O H
Cu on t-ZrO2